Structure and mechanism of chromatin remodeler SWI/SNF

A THESIS

SUBMITTED TO THE FACULTY OF THE GRADUATE SCHOOL OF THE

UNIVERSITY OF MINNESOTA

BY

Jinhua Wang

IN PARTIAL FULFILLMENT OF THE REQUIREMENTS

FOR THE DEGREE OF

MASTER OF SCIENCE

Dr. Aaron Goldstrohm, Advisor

December 2019

Acknowledgements

At the onset, I would like to express my gratitude to Dr. Aaron Goldstrohm for his assistance and guidance. I would like to thank him for helping me to make things go smoothly. I was grateful for his advice and feedbacks throughout my thesis. I am also very thankful to Dr. Zigang Dong who has been the supervisor of my graduate research for providing great support and guidance.

I would like to acknowledge my committee members Dr. Laurie Parker and Dr. Stephen Hecht for their constant guidance and encouragement throughout my graduate days. Thank their feedbacks on my thesis writing. I also would like to thank committee members Dr. Daniel Schmidt and Dr. Kevin Mayo for their guidance and assistance. I take this opportunity to thank Alyssa Callen for making sure I was on track with all the graduate school requirements.

I would like to thank my collaborator Dr. Junsheng Zhu who contributed to the work for nucleosome. Thank Bod Ashley who collected the cryo-EM data. Thank Dr. Hanyong Chen who worked on the data processing. Thank the support and equipment of Hormel Institute for contributing to the project. I would like to thank the lab members in Hormel Institute who provide great friendship and valuable discussions on research.

I would like to thank my parents and brothers for understanding and supporting me to chase my goal all the way. Thank my family for their unconditional love and support.

Lastly, I would like to give my thanks and gratitude to my husband for his endless love and encouragement.

Abstract

SWI/SNF complex, the ATP-dependent chromatin remodeler, alters the interactions between DNA and histones using the energy of ATP hydrolysis, modifying gene expression by controlling the accessibility of DNA to transcription factors. The gene-specific transcription is regulated through functional interactions within different subunits of SWI/SNF and associated co-factors. Genes encoding subunits of the SWI/SNF are mutated in more than 20% cancers, which has attracted a great deal of interest. Despite the huge amount of genetic, biochemical and structural biology data published, the mechanism by which SWI/SNF complex binds and remodels nucleosomes remains to be fully elucidated. High-resolution structure determination will certainly be invaluable for understanding the process in mechanistic detail. Given the dimensions, the complexity and the flexibility of the complex, single-particle cryogenic electron microscopy (cryo-EM) would be the optimal method of choice. However, it is difficult to purify and solve the structure of the whole multi-subunit macromolecular SWI/SNF complex. The highly conserved subunits, BRG1, BAF155, and BAF47 form a stable complex that retains nearly full remodeling activity and therefore have been regarded as the core components of SWI/SNF complex. Here we expressed the core sub-complex composed of BRG1, BAF155 and BAF47, with baculovirus expression system in Sf9 insect cells, and purified the complex with size exclusion chromatography. The result of negative staining electron microscopy showed that the protein sample of core SWI/SNF complex formed homogenous single particles after stabilization by Gradient Fixation (GraFix) method. We reconstituted nucleosome by wrapping

DNA around recombinant histone octamer and achieved nucleosome structure by cryo-EM. The core SWI/SNF complex had the capability to bind nucleosome assessed by electrophoretic mobility shift assay (EMSA). In future direction, the purified recombinant core SWI/SNF complex will be used for binding to reconstituted nucleosome and applied to cryo-EM for structure determination. Our work will illustrate the structure of chromatin remodeler engaging with its substrate, shedding light on the chromatin remodeling mechanism of SWI/SNF complex.

Table of Contents

List of Tables

List of Figures

List of Abbreviations

ARPs	Actin-related proteins
BAF	BRG1 associated factors
BAF155/170	BAF155 or BAF170
BAP	Brahma associated protein
bp	base pair
Cryo-EM	Cryogenic electron microscopy
EM	Electron microscopy
EMSA	Electrophoretic mobility shift assay
GraFix	Gradient Fixation
HSA	Helicase-SANT–associated
hSWI/SNF	Human SWI/SNF
H3K27me3	Trimethylation of histone H3 at lysine 27
H3K9Ac	Acetylation of histone H3 at lysine 9
IPTG	Isopropyl-β-D-1-thiogalactopyranoside
kDa	kilodaltons
MDa	Megadaltons
mSWI/SNF	Mammalian SWI/SNF
MW	Molecular weight
NCPs	Nucleosome core particles
PBAF	Polybromo-associated BAF
PBAP	Polybromo-associated BAP
PDB	Protein Data Bank
PRC	Polycomb repressive complex
SEC	Size exclusion chromatography
SHL2	Super-helical location 2
UF	Uranyl formate
2D	Two-dimensional
3D	Three-dimensional

Chapter 1 Introduction

1.1 Chromatin remodeling

Genomic DNA in eukaryotic cells wraps around the histone octamer, forming nucleosomes, the basic repeat unit of chromatin. The histone octamer is assembled by two copies each of histones H2A, H2B, H3 and H4 [1]. Linker DNA connects nucleosome core particles (NCPs) to create the classical 'beads on string' analogy used to describe the primary chromatin structure. The linker histone protein H1 binds to nucleosome at the DNA entry and exit site to stabilize nucleosome and facilitate higher-order chromatin structure [2, 3]. The chromatin assembly plays a central role in packing genetic material and maintaining genome integrity. However, the chromatin formation also creates a barrier to access DNA. Cells have evolved a set of chromatin remodeling factors to modulate chromatin structure. Chromatin remodelers are multi-subunits complexes that utilize the energy of ATP hydrolysis to slide, remove, and reconstruct nucleosomes, increasing the accessibility of DNA-binding proteins and transcription factors to DNA for regulating transcription, replication and repair [4]. Thus, chromatin remodelers play critical role in cellular replication and differentiation. The steps of remodeling include chromatin remodeler binding, disruption of histone–DNA contacts, the creation of a loop of DNA that propagates around the nucleosome in a wave-like manner. The consequences of remodeling reactions include: the repositioning of DNA with respect to the nucleosome (sliding) to expose a region

that was occluded previously; exchange of a standard histone with a variant histone; ejection of a nucleosome to expose associated DNA [5].

There are four families of chromatin remodeling complexes, including SWI/SNF, CHD, ISWI and INO80 [4]. The catalytic activity of each complexes depends on the activity of core ATPase subunit, with auxiliary subunits harboring DNA and histone-binding motifs. In each family of chromatin remodeling complexes, combinational subunit assembly provides extensive complex diversity [6]. The four families of chromatin remodelers share basic properties including: affinity for the nucleosome, domains that recognize covalent histone modifications, a similar ATPase domain (**Figure 1**), domains and/or proteins regulating ATPase domain, domains and/or proteins interacting with other chromatin or transcription factors. These shared properties allow nucleosome engagement, selection and remodeling [5].

Among the chromatin remodeler families, the most extensively mutated family is the mammalian SWI/SNF (mSWI/SNF) complex [6]. SWI/SNF remodelers are targeted to specific chromatin sites through histone modifications or a 'pioneering' DNA-binding protein. The remodeler then hydrolyzes ATP to conduct remodeling reactions, which lead to site exposure for an additional DNA-binding protein. The DNA-binding protein can be a repressor, an activator, or a regulator of chromosomal region. Thus SWI/SNF complexes remodel nucleosome construction and regulate gene expression [5].

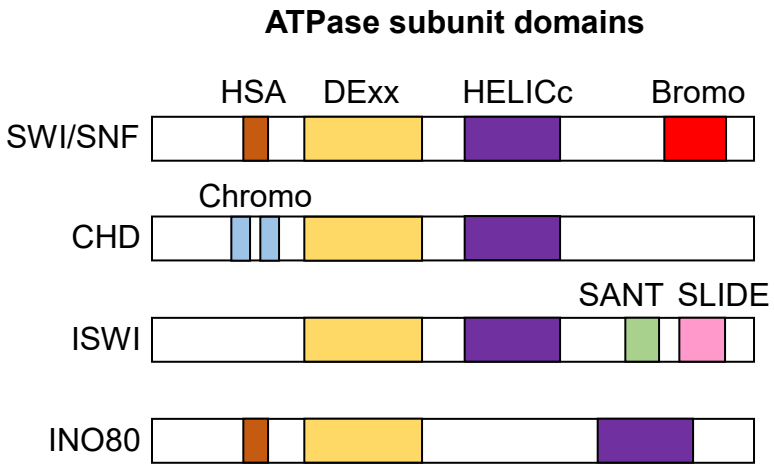

Figure 1. Domain organization within the ATPase subunit of each class of chromatin remodeling complexes (Derived from [6]).

All remodeling enzymes contain a shared ATPase domain and unique flanking domains. DExx and HELICc are shared domains with function of nucleic acid binding and ATP hydrolysis. Bromodomain recognizes acetylated lysines in histone tails. Chromodomain binds methylated lysines in histone tails. SANT and SLIDE domains recognized nucleosomes and internucleosomal DNA. HSA domain binds actin and actin-related proteins. HSA, helicase-SANT-associated; HELICc, helicase superfamily C-terminal; CHD, chromodomain helicase DNA-binding; SLIDE, SANT-like but with several insertions.

1.2 Evolutionary conservation of SWI/SNF complex

The SWI/SNF complexes were first characterized in yeast for mating-type switching and sucrose fermentation [7], then later characterized in *Drosophila* [8] and mammals [9]. They are highly conserved from yeast to human. SWI/SNF complex in *S. cerevisiae* yeast contains 11 subunits with a combined molecular weight over 1.5 MDa [10]. Another remodeling complex RSC identified in yeast, composed of 17 subunits, is highly similar to SWI/SNF [11]. As in yeast, the human and *Drosophila* contains two distinct remodeling complexes homologous to SWI/SNF and RSC, respectively. In *Drosophila*, the two complexes are named BAP (Brahma associated protein) and PBAP (Polybromo-associated BAP). In human, similarly, they are named BAF (BRG1 associated factors) and PBAF (Polybromo-associated BAF) (**Table 1**). The SWI/SNF and RSC complexes in higher eukaryotes retain some core subunits to maintain overall complex shape and remodeling activity, but also substitute or add other subunits with specific domains to accommodate increased genetic complexity.

Table 1. Conservation of SWI/SNF complexes during evolution (Derived from [12-14]).

Organism	Yeast		*Drosophila*		Human	
Complex	**SWI/SNF**	**RSC**	**BAP**	**PBAP**	**BAF (mSWI/SNF-A)**	**PBAF (mSWI/SNF-B)**
ATPase	Snf2	Sth1	BRM		BRG1 or hBRM	BRG1
Noncatalytic homologous subunits	Swi3	Rsc8	BAP155		BAF155 and BAF170	
	Snf5	Sfh1	BAP45		BAF47	
	Swi1		OSA		BAF250a/b	
		Rsc9		BAP170		BAF200
		Rsc1/2/4		Polybromo		BAF180
	Swp73	Rsc6		BAP60	BAF60a/b/c	
			BAP111		BAF57	
	Arp7	Rsc11	BAP47		β-Actin	
	Arp9	Rsc12	BAP55		BAF53a/b	
Unique	Swp82 Snf6 Snf11 Taf14 Rtt102	Rsc3-5,7 Rsc10,30 Ht11 Ldb7			BAF45a/b/c/d	
						BRD7

1.3 Subunits of mSWI/SNF complex

Mammalian SWI/SNF (mSWI/SNF) is a large complex containing more than 10 subunits with the molecular weight of over 1 MDa [15]. The modular organization of mSWI/SNF complexes was characterized, including canonical BAF complexes and PBAF complexes. BAF and PBAF share most of the same subunits and contain some specific subunits (**Table 1**) [15]. The mammalian complexes are composed of a catalytic ATPase subunit (either BRG1 or BRM), a set of highly conserved core subunits (BAF47, BAF155 and BAF170), and variant subunits that contribute to the targeting, assembly and regulation of lineage-specific functions of the complexes. The subunits of mSWI/SNF complexes are listed in **Table 2** with predicted molecular weight (MW) and function in complexes. The specific functions of several variant subunits are still unknown and need to be identified. The BRG1 and BRM subunits are mutually exclusive in the complexes, in which BRG1 is present in both BAF and PBAF complexes, whereas BRM is only in BAF complexes. The BAF250a and BAF250b subunits are mutually exclusive and are unique to BAF complexes, whereas BAF200, BAF180 and BRD7 subunits are unique to PBAF complexes. Several subunits (BAF60, BAF53 and BAF45) are encoded from different genes and have different isoforms, but only one of these can be incorporated into a cell- or tissue-specific remodeling complex. Thus, a large variety of SWI/SNF complexes exist in mammals and contribute to regulating lineage- and tissue-specific gene expression.

Table 2. Subunits of the mSWI/SNF complexes and their mutations in cancers (Derived from [15-18]).

Subunits	Gene (Alias)	MW (kDa)	Function	Associated cancers (mutation frequency)
BRG1	*SMARCA4*	184.5	ATPase and helicase catalytic subunit	Non-small cell lung cancer (35%), lung cancer, medulloblastoma (3%), burkitt lymphoma, SCCOHT
BRM	*SMARCA2*	181	ATPase and helicase catalytic subunit	Lung, colon, breast
BAF155	*SMARCC1*	123	Protein scaffolds, complex assembly	Small cell lung cancer (10%)
BAF170	*SMARCC2*	133	Protein scaffolds, complex assembly	Pancreatic cancer
BAF47	*SMARCB1 (hSNF5, INI1)*	44	Complex assembly, maintain integrity	Malignant Rhabdoid tumors (~98%), epithelioid sarcoma (~ 90%)
BAF250a	*ARID1A*	242	DNA binding	Ovarian clear cell carcinoma (57%), endometrioid carcinoma (35%), renal cell carcinoma, medulloblastoma, lung cancer; breast cancer, colon cancer, bladder cancer, neuroblastoma
BAF250b	*ARID1B*	236	DNA binding	Melanoma, neuroblastoma, hepatocellular, pancreatic, liver
BAF200	*ARID2*	197	DNA binding	Melanoma, hepatocellular carcinoma, pancreatic
BAF60a/b/c	*SMARCD1/2/3*	58/59/55	Unknown	
BAF57	*SMARCE1*	47	Unknown	Clear cell meningioma
β-Actin	*ACTB*	41.5	Unknown	

BAF53a/b	*ACTL6A/B*	47.5/47	Enhance ATPase activity	Squamous cell carcinoma
BAF45a BAF45b/c/d	*PHF10,* *DPF1/3/2*	56 42.5/43/44	Unknown	Colorectal cancer
BAF180	*PBRM1*	193	Unknown	Renal cell carcinoma (41%), breast cancer
BRD7	*BRD7*	74	Bind acetylated H3	Breast cancer

Numerous evidence have proved that BRG1, BAF155/170 and BAF47, form a stable complex that carries out essential chromatin remodeling activity and therefore have been regarded as the core components of SWI/SNF complex [13, 17, 19, 20]. BAF155/170 and BAF47, stimulate the remodeling activity of catalytic subunit BRG1 in vitro [19]. They are highly conserved subunits found in all characterized SWI/SNF family complexes from yeast through humans [15].

As the essential ATPase and helicase catalytic subunit, BRG1 protein contains the catalytic core domain, N-terminus and C-terminus. The domain architecture and function of each domain are shown in **Figure 2** and **Table 3**. The catalytic core domain binds to ATP, hydrolyzes ATP to provide energy, and binds nucleosomal DNA and histone tail to initiate remodeling reaction. The N-terminus mediates protein interactions with transcription factors and other subunits in complex. The C-terminus interacts with histones to regulate remodeling activity [21].

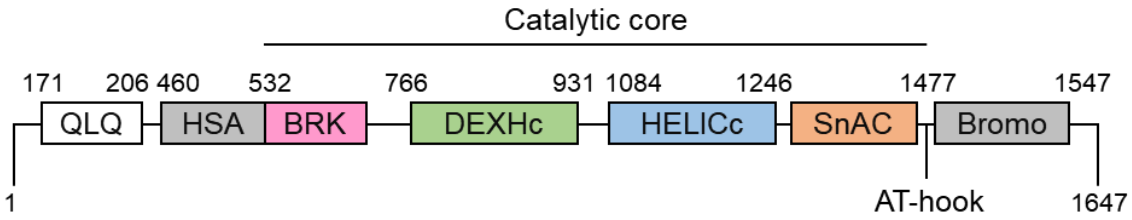

Figure 2. Architecture of BRG1 domains.

Table 3. Functions of BRG1 domains (Derived from [21]).

Domain	Putative Function
QLQ	Conserved Gln-Leu-Gln motif. Mediate protein-protein interactions.
HSA	Bind to actin.
BRK	Associated with helicases and transcription factors.
DEXHc	ATP-binding region.
HELICc	ATP-hydrolysis.
SnAC	Binds histones
AT-hook	A small DNA-binding protein motif.
Bromo	4-helix motif. Interact specifically with acetylated lysine.

BAF155 and BAF170 function as complex scaffolds and maintain complex assembly [17]. The domain architecture of BAF155 is shown in **Figure 3**. BAF155 has 68% identity with BAF170 of protein sequence, and their protein sequences are highly conserved (**Figure 4**), so BAF170 and BAF155 have same domain structure. These two members can dimerize in solution and appear to make hetero- (155/170) or homodimers (155/155 or 170/170) within the complexes in mammalian cells [22]. The 155/155 homodimers are found in embryonic stem cells (ESCs) and 155/170 heterodimers in most differentiated cell types [23]. As reported, removal of both BAF155 and BAF170 subunits resulted in near-complete degradation of all mSWI/SNF complex components, supporting the role for the BAF155 and BAF170 as the platform for mSWI/SNF formation [23]. Besides high structural similarity, BAF170 and BAF155 have same function in complex. The loss of BAF155 and BAF170 in double-conditional knockout (dcKO) mice leads to the dissociation of all other BAF subunits from the complex, resulting in an overall reduction in active chromatin marks (H3K9Ac), a global increase in repressive marks (H3K27me2/3), and downregulation of gene expression [24]. Subsequently, the free BAF subunits are degraded by the ubiquitin-proteasome system [24]. In summary, BAF155 and BAF170 are indispensable to the integrity of SWI/SNF complexes.

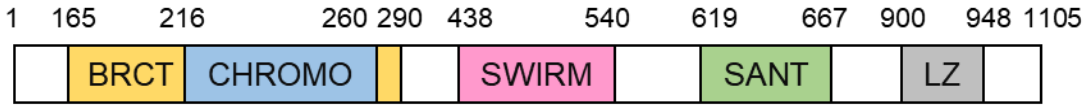

Figure 3. Domain architecture of BAF155 (Derived from [25]).

BRCT (BRCA1 C-terminal) domain can bind the phosphate from DNA. CHROMO domain is associated with chromatin targeting. SWIRM (SWI3, RSC8, and MOIRA) domain can bind nucleosomal DNA. SANT (SWI3, ADA2, N-CoR, and TFIIIB) domain, is DNA binding domain. LZ (leucine zipper) domain is DNA binding domain.

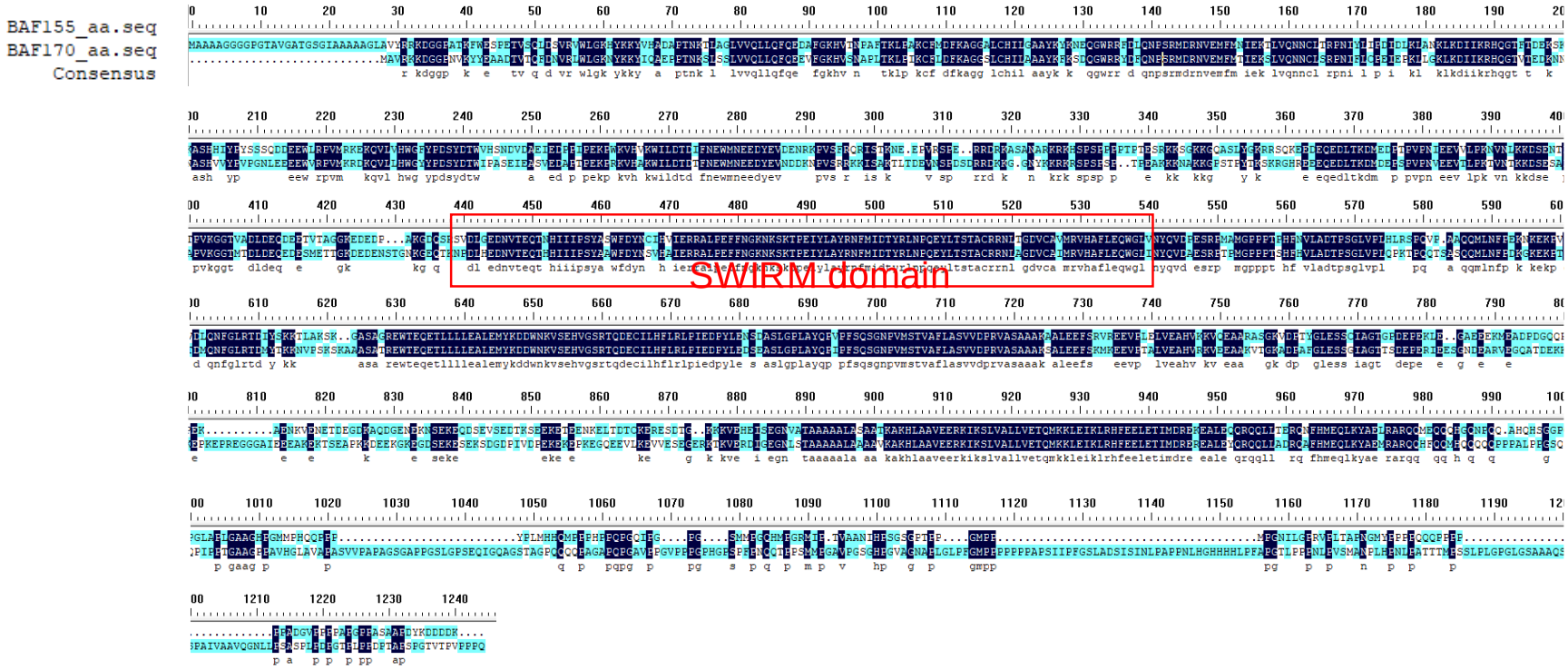

Figure 4. The protein sequence of BAF155 has 68% identity with BAF170.

The sequence alignment was performed using DNAMAN software. Conserved amino acids in both proteins are highlighted in black. SWIRM domain was indicated with red rectangle.

BAF47 has the key role in maintaining complex assembly and integrity [17]. Loss of BAF47 induces formation of an aberrant SWI/SNF complex, resulting in transcription defects [26]. The domain architecture of BAF47 is shown in **Figure 5**. The structural study has proved that BAF155 SWIRM domain binds directly to BAF47 the repeat 1 (RPT1) domain [25]. BAF155 SWIRM shares over 95% sequence identity with BAF170 SWIRM (**Figure 4**), and all residues important for RPT1 binding are highly conserved [25]. Thus, BAF170 SWIRM domain binds equally well to BAF47 RPT1. Moreover, BAF47 interacts with the ATPase domain of BRG1 and promotes its binding to DNA. BAF47 also contacts the surface of the H2A-H2B dimer in nucleosomes. In addition, BAF47 is essential for SWI/SNF recruitment by transcription factor [26].

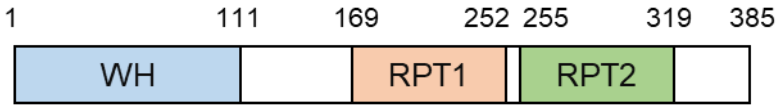

Figure 5. Domain architecture of BAF47 (Derived from [25]).
WH (winged helix) domain is DNA binding domain. The repeat domains (RPT1 and RPT2) can bind proteins.

1.4 mSWI/SNF complex and cancer

Genes encoding subunits of the SWI/SNF complex are mutated in more than 20% cancers [27] and subunits are frequently mutated in a variety of cancers (**Table 2**) [15]. SWI/SNF complex activates gene expression through its ability to remodel and evict nucleosome at gene promoters or enhancers [28]. The alterations of

SWI/SNF complex cause defective complex assembly and recruitment, abnormal gene silencing including tumor suppressor, which results in tumor development [15, 29].

Several studies have reported the mechanisms about the role of SWI/SNF complex in controlling gene expression and suppressing tumor development. *SMARCB1* gene, encoding BAF47 subunit, is inactivated in approximately 98% of malignant rhabdoid tumor [30, 31]. In the study of Charles Roberts and colleagues [32], the genome location of SWI/SNF in wide-type cells and *SMARCB1*-deficient rhabdoid tumor cells was compared. They found that SWI/SNF was recruited to promoters, typical enhancers and super-enhancers (cluster of multiple enhancers) in wild-type cells. Loss of *SMARCB1* caused that most of SWI/SNF complex disassembled at promoters and typical enhancers region, however, SWI/SNF at super-enhancers were much less affected. As the authors proposed, typical enhancers regulate genes related to lineage specification whereas super-enhancers regulate genes involved in cell identity. Thus, in *SMARCB1*-deficient cells, the redistribution of SWI/SNF impairs cell differentiation whereas maintains cell abilities of self-renewal, survival and proliferation, promoting tumorigenesis [28]. In another study of Charles Roberts and colleagues [33], they focused on the inactivation of *ARID1A* gene encoding BAF250a subunit. BAF250a, the most frequently mutant subunit in SWI/SNF complex, functionally binds DNA and guides SWI/SNF to target gene promoters or enhancers for chromatin remodeling [34]. They found that *ARID1A* knockout in mouse colon tissues caused colon tumorigenesis. *ARID1A* loss impaired SWI/SNF recruitment at promoters and

enhancers, which in turn down-regulated gene expression. In summary, these two studies identify the role of SWI/SNF complex at gene promoters, but also enhancers and super-enhancers. These also potentially explained why mutations in SWI/SNF complex caused cancers.

The molecular connection between abnormal SWI/SNF activity and deregulated gene expression was explained by the genetic antagonism between SWI/SNF complex and Polycomb repressive complex (PRC). PRC promotes transcriptional silencing and SWI/SNF complex has the function of opposing PRC to activate gene expression [35]. In normal cells, the antagonism between SWI/SNF complex and PRC maintains the balance between differentiation and self-renewal. However, defects in SWI/SNF can break the balance, impairing differentiation and promoting self-renewal for tumorigenesis. In the study of Gerald Crabtree and colleagues [36], they found that inactivation of *SMARCA4* gene, encoding the ATPase subunit BRG1, increased the localization of PRC on the genome. Moreover, *SMARCA4* inactivation caused the enrichment of trimethylation of histone H3 at lysine 27 (H3K27me3) that is gene silencing marker mediated by PRC, resulting in the down-regulation of gene expression. Wild-type SWI/SNF complex interacts with PRC and evicts PRC from chromatin [37]. *SMARCA4* loss results in decreased chromatin affinity of SWI/SNF, defective enhancer activation, and inability to oppose PRC-mediated repression at promoters [32, 38]. Recent studies indicate that loss of *SMARCB1* or *ARID1A* exhibit mechanistic convergence with *SMARCA4* loss [39]. The further characterization of SWI/SNF-mediated PRC eviction from chromatin by using

purified proteins would be critical to understand the biochemical mechanisms. It has been proved that pharmacological inhibition of PRC could be a therapeutic strategy for SWI/SNF-inactivated cancers [40].

1.5 Structural studies related to SWI/SNF complex

Despite the functional importance, the structural information of SWI/SNF complex was still limited to low-resolution electron microscopy (EM) reconstruction without detailed subunits localization and SWI/SNF-nucleosome structure. The low-resolution 3D reconstruction showed that subunits of SWI/SNF form a large cavity with about 15 nm in diameter and about 5 nm in depth, which make this cavity an excellent candidate for a potential nucleosome-binding pocket [41-43].

Until now, partial structures of several subunits in yeast SWI/SNF complex were identified. The structure of a four-protein subcomplex within SWI/SNF that consists of Snf2 HSA domain, Arp7, Arp9, and Rtt102 has been characterized by crystallography [44]. The ARPs (actin-related proteins, Arp7 and Arp9) contact the HSA (helicase-SANT–associated) domain of the catalytic ATPase subunit Snf2 and are thought to regulate ATPase activity. Arp7 and Arp9 pack together and straddle the HSA domain. Rtt102 wraps around one side of the complex in a highly extended conformation that contacts both ARPs and therefore stabilizes the complex (**Figure 6**). This structure provides the mechanisms of ARPs interacting with ATPase subunit.

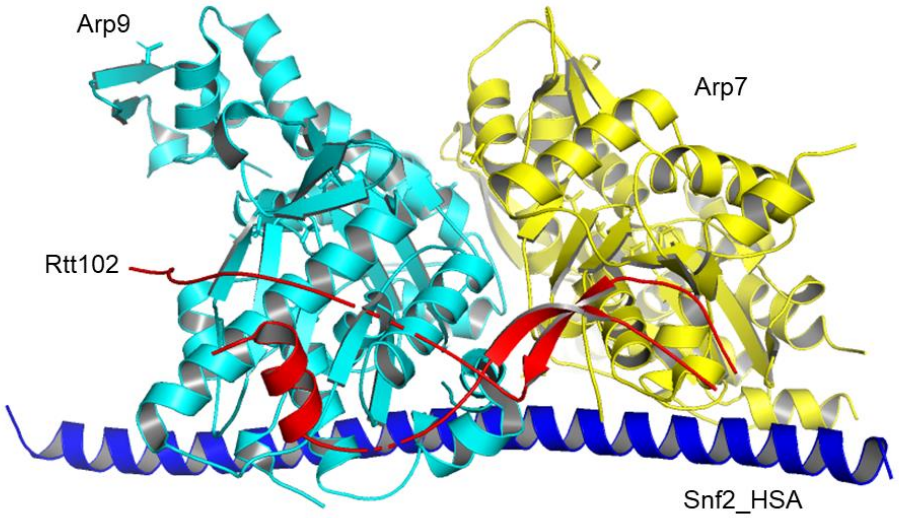

Figure 6. Structure of Arp9-Arp7-Snf2_HSA-Rtt102 subcomplex of SWI/SNF chromatin remodeler (Derived from PDB: 4I6M). Arp9, cyan; Arp7, yellow; Snf2_HSA, blue; Rtt102, red.

The catalytic core domain structure of Snf2, the yeast homologue of human BRG1, has been identified by crystallography [45]. Structure and mechanism of Snf2 catalytic core domain bound to nucleosome also has been identified by cryo-EM in the same research group [46, 47]. Snf2 binds to SHL2 (super-helical location 2, at the side proximal to the linker DNA, the entry point of nucleosome) and the proximal H4 tail of nucleosome (**Figure 8**), which contacts a highly negatively charged surface of the catalytic domain (acidic surface). Binding to H4 tails strengths the remodeling activity of Snf2. ATP binding and hydrolysis would then induce closure of catalytic core domain and deliver 1 bp of the DNA at SHL2 towards the dyad, initiating the remodeling reaction. This mechanism of DNA translocation by Snf2 is consistent with the notion that the ATPase domain of the

remodeler is an autonomous machine, and it remodels the nucleosome 1-2 bp at a time. A ‘wave–ratchet–wave’ model for chromatin remodeling was proposed, in which a tracking subdomain remains bound at a fixed position on the histone octamer, and a torsion subdomain undergoes a conformational change and pulls the DNA [47]. A ‘twist diffusion’ model explains the propagation of DNA distortion along the histone surface; catalytic core domain binds to SHL2 position and pulls DNA from entry to exit side, causing wave or twist of DNA; then the twist diffuses to exit side, resulting in DNA translocation [47].

The structure of human BRG1 bromodomain has been identified by crystallography. Bromodomain consists 4 helixes (**Figure 7**) [48] and can bind DNA and acetylated histone tail [49]. In addition, the SWIRM domain of BAF155 subunit binds directly to the RPT1 domain of BAF47 subunit and the structure has been identified by crystallography (**Figure 9**) [25]. This provides evidence for the interaction between BAF155 and BAF47 within SWI/SNF complex.

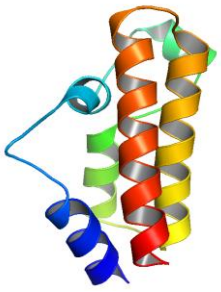

Figure 7. Structure of Human BRG1 bromodomain (Derived from PDB: 2H60).

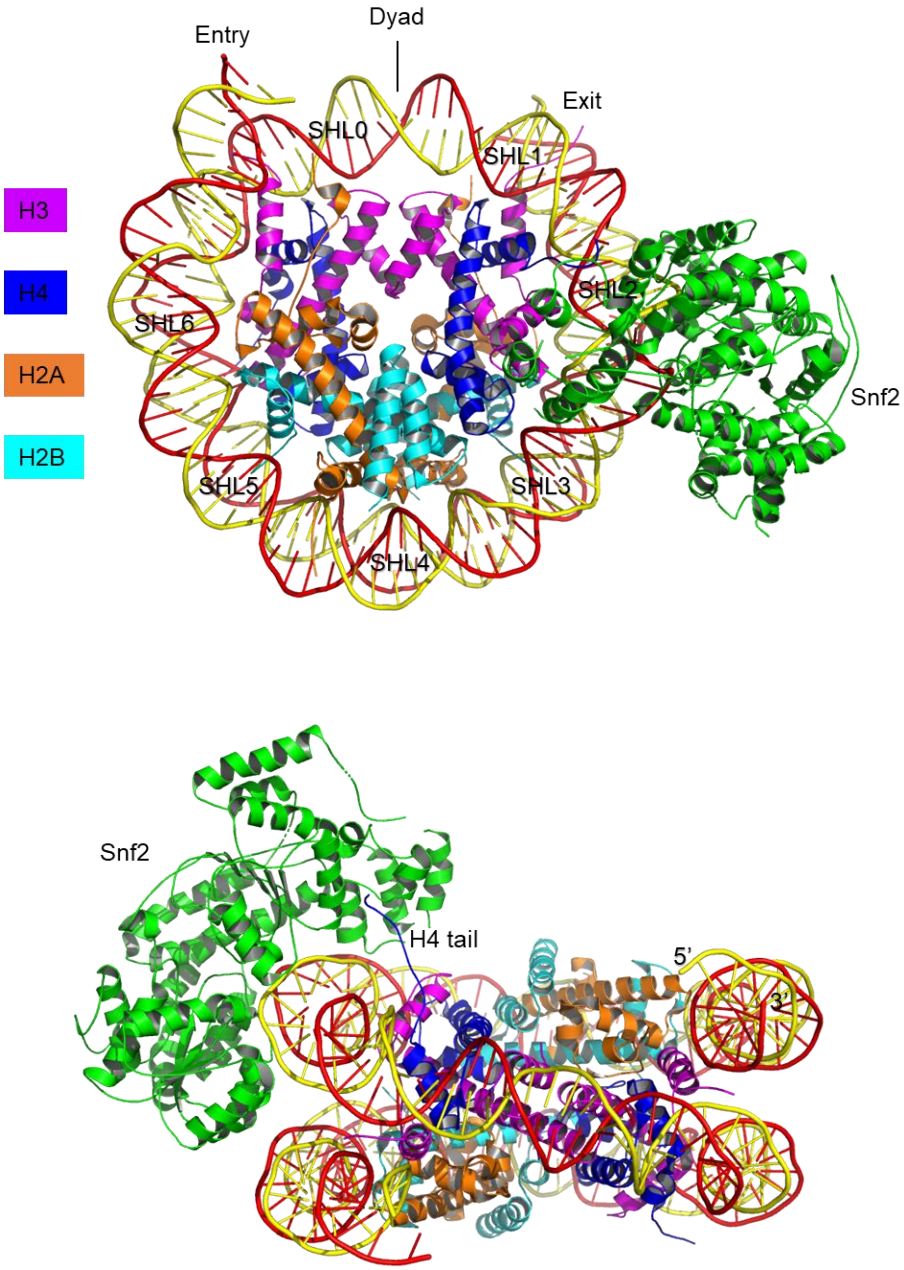

Figure 8. Overall structure of Snf2 bound to nucleosome around SHL2 and H4 tail (Derived from PDB: 5X0Y).

Top view (up) and side view (down) of the cryo-EM density map of Snf2 bound to nucleosome. Snf2, green; histone H3, magenta; H4, blue; H2A, orange; H2B, cyan; 5'-DNA, yellow; 3'-DNA, red. The DNA had 167 base pairs.

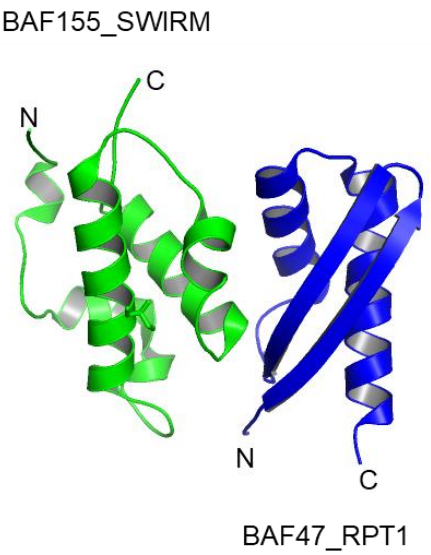

Figure 9. Structure of BAF155 SWIRM domain bound to BAF47 RPT1 domain (Derived from PDB: 5GJK).

The heterodimer of SWIRM and RPT1 was formed by electrostatic and hydrophobic interactions. BAF155 SWIRM domain, green; BAF47 RPT1 domain, blue.

Considering the compositional complexity and the associated relative structural instability of SWI/SNF complex, despite the huge amount of genetic, biochemical and structural biology data published, the mechanism by which SWI/SNF complex binds and remodels nucleosome remains to be fully elucidated. High-resolution structure determination will certainly be invaluable for understanding the process in mechanistic detail. Thus, the improved three-dimensional (3D) EM reconstruction of SWI/SNF-nucleosome complex is critical to illustrate the subunits architecture and remodeling mechanism.

1.6 Research goal and significance

Our research aims to uncover the structure and mechanism of SWI/SNF in chromatin remodeling. Our work will illustrate the structure of chromatin remodeler engaging with its substrate, shedding light on the chromatin remodeling mechanism of SWI/SNF complex, explaining how remodelers bind their substrates and initiate remodeling reaction. Moreover, since BRG1 has the role of suppressing tumor and is highly mutated across a broad range of human cancers [50-53], our work about the structure and mechanism of BRG1 would provide more details for its role on regulating gene expression and provide the basis for exploring rational cancer therapy. For example, BRG1 is mutually exclusive in SWI/SNF complexes with its paralogue BRM [54]. BRM-containing SWI/SNF complexes were intact in BRG1-loss cells and the proliferation of these cells was impaired by BRM knockdown [54]. Remarkably, BRM is a synthetic lethal vulnerability in BRG1-mutant human cancer [55]. Thus, BRM can be the cancer therapy target in BRG1-mutant human cancer [56]. Our work about the BRG1 protein structure would be the basis for discovering the subunit-specific inhibitors targeting BRM in the future by exploring the structure difference between these two subunits (BRG1 and BRM) for the treatment of BRG1-mutant human cancer without impairing the non-mutant normal cells. Therefore, the identification of high-resolution 3D structure will largely potentiate the rational design and discovery of small-molecule inhibitors.

Given the dimension of the complex, single-particle cryogenic electron microscopy (cryo-EM) would be the appropriate way to study the structure of

complex. Cryo-EM is the most feasible way to identify the structure of macromolecular complex without the need for crystals and can reach near-atomic resolution (< 4 Å) [57]. However, it is difficult to purify and solve the structure of whole macromolecular SWI/SNF complex with multiple subunits and compositional complexity. It has been proved that BRG1, BAF155/170, and BAF47, form a stable core sub-complex that carries out essential chromatin remodeling activity [19]. The cross-linking mass spectrometry (XL-MS) results demonstrates the direct binding and close interaction within BRG1, BAF155/170 and BAF47 [26]. The detailed structural information of core SWI/SNF complex bound with nucleosome would explain the remodeling mechanism.

Chapter 2 Structure of core SWI/SNF complex

2.1 Introduction

BRG1, BAF155/170 and BAF47, form a stable complex that retains nearly full remodeling activity and therefore have been regarded as the core components of SWI/SNF complex [19]. To purify the core complex, Baculovirus expression system was applied, which generates baculovirus for high-level expression of recombinant protein [58]. Firstly, each subunit was prepared with individual baculovirus for respective expression. Our results showed that BRG1, BAF155 and BAF170 could be expressed at high levels by itself, however, the expression level of BAF47 itself was very low. It has been reported that BAF155 can interact with and stabilize other subunits of SWI/SNF by protecting them from proteasomal degradation [59]. BAF155 interacts with and stabilizes BAF47 by attenuating its proteasomal degradation through blocking its ubiquitination by preventing interaction with the E3 ubiquitin ligase [60]. Thus, BAF155 and BAF47 were co-expressed by cloning into single baculovirus. We observed that expressing BAF155 resulted in an increase of BAF47.

Considering the dimension of core SWI/SNF complex, single-particle cryogenic electron microscopy (cryo-EM) would be the optimal way to determine the structure of this macromolecular complex at near-atomic resolution without the need of crystals. In cryo-EM, sample is embedded in an aqueous environment by applied to a meshed grid and plunge freezing in liquid ethane. Electrons interact strongly with atoms of protein sample, so that the molecules within the specimen

are imaged directly. The density of biological molecule was reconstructed from a set of 2D projections of the molecules imaged at various orientations by the electron microscope [61].

A single-particle cryo-EM project should start with the characterization of specimen in negative-staining EM, which is a beneficial way to assess sample concentration, sample homogeneity, protein stability, protein particle size and shape [62]. Negative staining involves the addition of a heavy metal salt stain that forms an electron-dense mold around individual macromolecular complexes. Electron beam is deflected by interacting with heavy metal ions in stain, producing phase contrast. Since the stain is excluded by protein sample, deflection of electron beam through protein sample is much less than through stain rich regions [62]. In negative staining EM, electron-dense mold produces a high contrast image and is resistant to radiation damage [63]. Thus, negative staining EM is the preferred method for optimizing samples by checking the particle distribution, integrity and concentration. Moreover, negative staining can also be applied for low-resolution structure determination to get an initial model. Once the ideal conditions for protein sample determined, sample will be frozen for cryo-EM imaging by the way of plunge freezing.

Plunge freezing results in a sample that is preserved in a physiological buffer, thus preserving not only its native conformation but also high-resolution structural information [64]. For this technique, samples are pipetted onto an EM grid, and after blotting away excess solution, the grid is then plunged into liquid ethane. This procedure vitrifies the aqueous solvent, thus preserving the

hydrogen-bonding networks that normally surround a macromolecule in liquid water. Freezing must be rapid enough to prevent ice crystal formation. Finally, prepared grids are subjected to cryo-EM imaging. Samples are visualized at low temperatures, to preserve the samples in a vitrified state, and to provide them some protection from the noxious effects of the electron beam. Single particles are picked from cryo-EM images for data processing, in order to establish the density map for protein structure determination.

A macromolecular complex might dissociate during EM grid preparation. GraFix (Gradient Fixation) method is a beneficial way to purify and stabilize macromolecular complexes for single particle cryo-EM. During GraFix, macromolecules undergo a weak, intramolecular chemical cross-linking while being purified by density gradient ultracentrifugation [65]. Sample is centrifuged into a combined glycerol and glutaraldehyde (cross-linking regent) gradient (**Figure 10**). Following ultracentrifugation, samples are fractionated from bottom to top with capillary tube and peristaltic pump. The protein sample stabilized by GraFix can be directly applied to negative staining or unstained cryo-EM after changing buffer to remove glycerol. It has been proved that this method significantly reduced the problems of heterogeneity resulting from complex particle dissociation during EM grid preparation. In addition, this method increases the particle binding to the carbon support film of grids, without apparent disruption of native structure of complex [65]. In summary, these benefits make GraFix an appropriate choice to stabilize macromolecular complex to improve sample homogeneity for EM sample preparation.

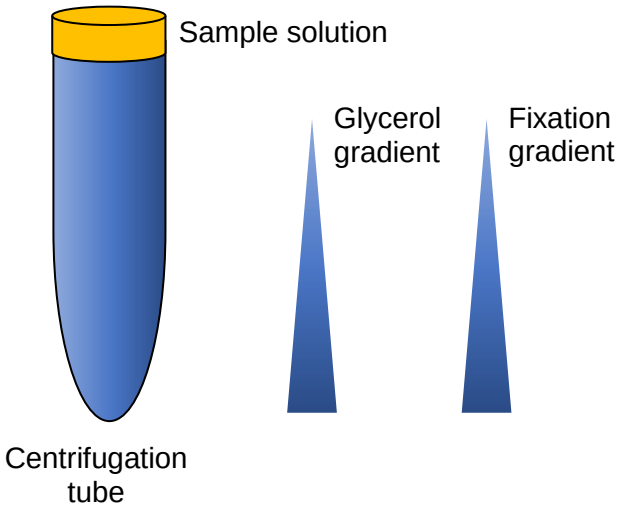

Figure 10. The GraFix method (Derived from [65]).

The centrifuge tube contains glycerol gradient and fixation gradient with cross-linking regent. Protein sample is loaded onto the top in the centrifuge tube. This method combines purification by ultracentrifugation with cross-linking through increasing exposure to cross-linking regent.

In this chapter, we aimed to purify the core SWI/SNF complex and applied the complex to cryo-EM for structure determination. The core SWI/SNF complex composed of BRG1, BAF155, and BAF47 was purified from Sf9 insect cells infected with baculoviruses by anti-Flag M2-agrose beads and size exclusion chromatography. We concluded that BRG1, BAF155, and BAF47 formed stable core SWI/SNF complex. The negative staining EM result of the complex showed homogenous particles after the GraFix stabilization, and the specimen could be applied to cryo-EM for data collection and data processing for structural determination.

2.2 Materials and Methods

2.2.1 Protein expression

To co-express BAF47 and BAF155 or 170, the genes of BAF47 and BAF155 or 170 were cloned into the vector of pFastBac Dual, which contains two strong baculovirus promoters (polyhedrin and p10) to allow simultaneous expression of two proteins and two large multiple cloning sites for simplified cloning. The gene of BRG1 was cloned into pACEBac1 vector to make baculovirus for expression. The recombinants plasmids were generated by cloning genes of interest into corresponding vectors using restriction enzyme digestion and ligation, and then transforming into DH5α competent cells. Then the made constructs containing genes of interest were transformed into DH10EMBacY competent cells for transposition into the bacmid. The EMBacY backbone contains a constitutively expressing YFP expression cassette which allows for easy monitoring of viral titer via fluorescence. Then, blue/white selection identifies colonies containing the recombinant bacmid. The bacmid DNA containing the gene of interest from DH10EMBacY was purified and used in Sf9 insect cell transfection with Cellfectin™ II transfection regent (Gibco) to produce recombinant baculovirus. The P0 virus was released into the medium after 96 hours transfection and harvested from the cell culture medium. The small-scale, low-titer P0 virus was used to infect cells to generate a high-titer P1 stock. Then P1 stock was used to scale up the amplification procedure to produce high-titer P2 and P3 stock by scaling up the number of cells and volume of virus that is used appropriately. The high titer baculovirus stock was used to infect insect cells for recombinant protein

expression. The insect cell line Sf9 was cultured in serum-free conditions with suspension culture using the medium Sf-900™ III SFM. Cells were cultured in a 27°C humidified incubator. The cells were infected by baculovirus stock when cells are in the mid-logarithmic phase growth at a density of 1×10^6 to 2×10^6 cells/mL. Cells were harvested 72 hours post-infection with maximum protein expression. Cell lysate was collected. Protein expression was analyzed by SDS-PAGE and western blot.

2.2.2 Protein purification

Sf9 insect cells grown in suspension were coinfected with equal volumes of two baculovirus stocks, with one baculovirus containing the genes for expressing 3 × Flag (DYKDHDGDYKDHDIDYKDDDDK) -tagged BRG1, the other baculovirus containing the genes for expressing BAF47 and BAF155/170. Time courses of expression were performed to determine the conditions where maximal amount of BRG1, BAF47 and BAF155/170 could be expressed. Cells were harvested around 72 hours post-infection and cell pellet was collected. Because SWI/SNF complex functions in cell nucleus, nuclear extracts were isolated to purify the protein complex as described [19]. Cell pellets were suspended in hypotonic buffer (10 mM HEPES [pH 8.0], 10 mM KCl, 0.1 mM EDTA, 1 mM DTT, 0.5% Tween-20, 1 mM PMSF along with protease inhibitors] and allowed to swell on ice for 20 min with intermittent mixing. Nucleus was collected by centrifugation for 10 min at 4000 rpm in a JS-4.2 rotor. The pelleted nucleus was resuspended in the nuclear extraction buffer (20 mM HEPES [pH 8.0], 500 mM NaCl, 10% glycerol, 1 mM

EDTA, 1 mM DTT, 1% Tween-20, 1 mM PMSF along with protease inhibitors) and allowed to extract for 30 min with continuous gentle mixing. Nuclear extract was collected by centrifugation for 30 min at 12,000 rpm in a JA-20.1 rotor. Protease inhibitor cocktail used throughout the extraction procedure were 50 μM PMSF, 10 μM pepstatin A, 20 μM leupeptin, 100 μM benzamidine and 50 μM bestatin. Nuclear extracts were incubated with anti-Flag M2-agarose beads (Sigma) at 4 ℃ overnight. Beads were then washed with washing buffer (20 mM HEPES [pH 8.0], 300 mM NaCl, 10% glycerol, 0.1% Tween-20). Proteins were eluted from beads in washing buffer with 100 μg/mL 3 × flag peptide and 2 mM TCEP. Then the protein samples were concentrated and loaded onto Superose 6 5/150 GL or 10/300 GL size exclusion chromatography column (GE Healthcare), pre-equilibrated in buffer containing 20 mM HEPES [pH 8.0], 300 mM NaCl and 1 mM DTT. The fractions were collected every 200 μL, examined by SDS-PAGE and gel was stained with coomassie brilliant blue. Central peak fractions were pooled and concentrated for EM sample preparation.

2.2.3 Negative staining EM

Negative-staining samples were prepared using 0.75% uranyl formate (UF) dissolved in 12.5 mM NaOH. Firstly, holey grids coated with continuous carbon film were glow discharged for 10 seconds, and then 3 μL of sample were pipetted on the grid. Sample stayed on grid for 60s, then grid was blotted by filter paper to remove excess protein solution and washed with water for three times. The stain of 0.75% UF was added to the grid and stayed for 15 seconds. Then the excess

stain was blotted by filter paper and grid was dried in air. The grids with sample were observed using a 120 kV Tecnai F20 microscope (FEI) equipped with a Gatan Ultrascan 4000 camera at a magnification of ×49,000.

2.2.4 GraFix

GraFix (Gradient Fixation) is a method to stabilize macromolecular complexes for single particle cryo-EM. During GraFix, macromolecules undergo a weak, intramolecular chemical cross-linking without apparent disruption of the native structures while being purified by density gradient ultracentrifugation [65]. We purified and stabilized the core SWI/SNF complex using the GraFix. To form the gradient, top solution containing 20 mM HEPES [pH 8.0], 300 mM NaCl, 2 mM DTT and 10% glycerol (Sigma) was added to a tube (Beckman, 331372). Bottom solution containing 20 mM HEPES [pH 8.0], 300 mM NaCl, 2 mM DTT, 30% glycerol and 0.15% glutaraldehyde (Polysciences) was then injected to the bottom of the tube using a syringe with a blunt-ended needle. The tubes were placed into a gradient master (BioComp) to form a continuous density and glutaraldehyde gradient. Finally, 200 µL (100 µg) of sample were loaded on the top of tube. The sample tubes were ultra-centrifuged at 4°C for 15 hours at a speed of 33,000 rpm (Beckman, Rotor SW-41Ti). Following ultracentrifugation, fractions were collected every 200 µL from bottom to top. Tris buffer [pH 8.0] was added to quench cross-linking reaction when fractions were being collecting. Then fractions were examined by 6% SDS-PAGE gels. The gels were stained with coomassie brilliant blue. The central peak fractions were selected, pooled and subjected to desalting

column with buffer (20 mM HEPES [pH 8.0], 300 mM NaCl, 2 mM DTT) for buffer exchange to remove glycerol in sample. Finally, sample was concentrated for EM sample preparation.

2.2.5 Cryo-EM

For cryo-EM sample preparation, a drop of 4 µL sample was applied to a glow-discharged Quantifoil holey carbon grid (R1.2/1.3, 300 mesh). After waiting for 60s, the grid was blotted for 4.0s (under 95% humidity and 4℃) and plunged into liquid ethane cooled by liquid nitrogen using FEI Vitrobot. The samples were observed using a Titan Krios microscope (FEI) operated at 300kV, equipped with a Gatan K2 Summit camera, which is a direct detection camera with the highest performance detector available for cryo-EM. Then micrographs were achieved.

2.2.6 Nucleosome binding assay

The nucleosome binding affinity was assessed through electrophoretic mobility shift assay (EMSA). The purified protein sample of core SWI/SNF complex was dialyzed against 20 mM HEPES, 60 mM NaCl, pH 7.8. 20 µM nucleosome was incubated with increasing amount of core SWI/SNF complex from 1 µM to 20 µM, 3 mM ADP, 3 mM $BeSO_4$, 10 mM NaF and 10 mM $MgCl_2$, in which ADP•BeF_3 produced was ATP analogue and Mg^{2+} was beneficial for nucleosome binding. After incubation on ice for 30 min, the samples were resolved by electrophoresis on 4.0% native TBE polyacrylamide gels at 70V for 90min at 4 ℃. The gels were stained with SYBR Gold nucleic acid gel stain (Thermo Fisher Scientific) and

imaged. The bound fractions are assessed based on the disappearance of free NCPs relative to the intensity of the entire lane.

2.3 Results

2.3.1 Expression and purification of core SWI/SNF complex

All four proteins of BRG1, BAF47, BAF155 and BAF170, were co-purified by immunoprecipitation based on the Flag epitope. BRG1 tagged with 3 × Flag tag pulled down the other subunits of BAF155, BAF170, and Halo-tagged BAF47, indicating the interactions within these subunits (**Figure 11**). However, the intensity ratio of BAF155 and BAF170 protein bands were variable based on coomassie brilliant blue staining. This was probably because that BAF155 and BAF170 formed heterodimer (155/170) or homodimers (155/155 or 170/170) within the SWI/SNF complexes, so that amount of BAF155 to BAF170 was not equal if their recombinant protein expression amounts were not same. Given that BAF155 and BAF170 have highly similar protein structure and same function in the complex, either BAF155 or BAF170 instead of both would be included in the core SWI/SNF complex reconstitution. The results showed that BRG1, BAF47, BAF155 or BAF170, formed stable complex in vitro (**Figure 11**). The protein samples were loaded to Superose 6 5/150 GL size exclusion column with a bed volume of 3 mL, which was applied to characterize protein sample with less amount in the small-scale test experiment. The size exclusion chromatography (SEC) results demonstrated that peaks of the complexes of BRG1+BAF170+BAF155+BAF47, BRG1+BAF170+BAF47, BRG1+BAF155+BAF47 were at the nearly same position

of elution volume (**Figure 12**), indicating that these complexes had nearly same size, consistent with the hypothesis that these complexes had same composition except for the replacement between BAF155 and BAF170. To avoid the interference of Halo tag (with a molecular weight of 33 kDa) to the protein structure, the baculovirus containing the genes of untagged BAF47 and BAF155 was generated and small-scale test results of protein purification showed that BRG1, BAF155, and BAF47 formed a stable complex (**Figure 13**).

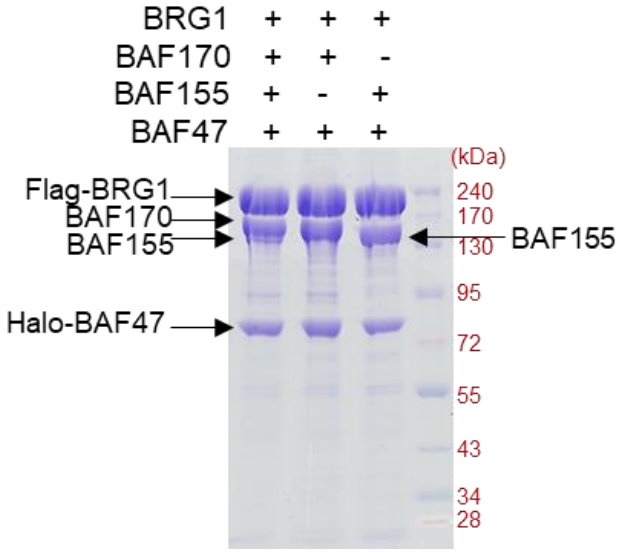

Figure 11. Purification of core SWI/SNF complex composed of BRG1, BAF47, BAF155 and/or BAF170.

Sf9 cells were co-infected with baculoviruses for expressing Flag-tagged BRG1, Halo-tagged BAF47, untagged BAF155 and/or BAF170. Cells were harvested 72 hours post-infection. Cell lysate was incubated with anti-Flag M2-agarose beads. Elution from beads was analyzed with SDS-PAGE and gel was stained with coomassie brilliant blue.

A

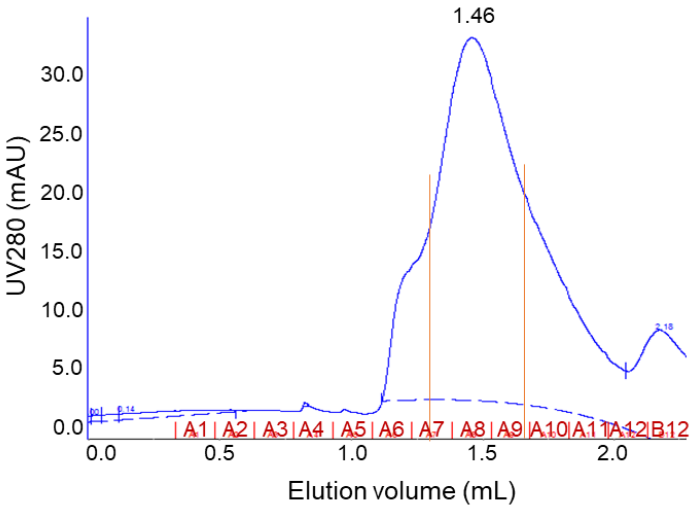
B17015547 Superose 6 5/150
1.46
30.0
25.0
20.0
15.0
10.0
5.0
0.0
UV280 (mAU)
A1 A2 A3 A4 A5 A6 A7 A8 A9 A10 A11 A12 B12
0.0
0.5
1.0
1.5
2.0
Elution volume (mL)

B

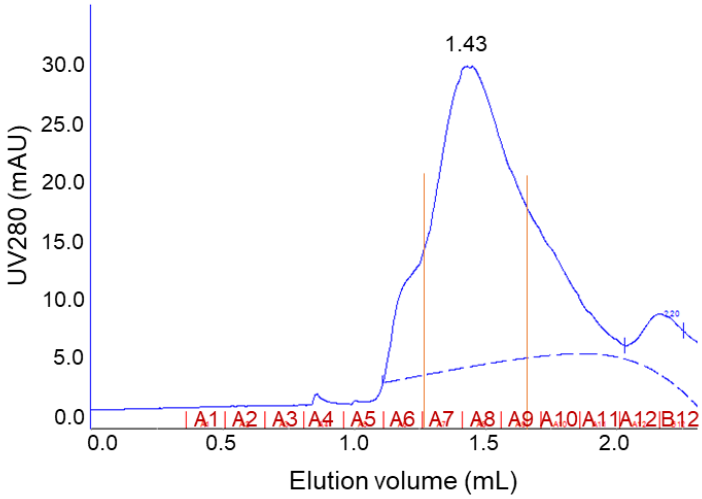
B17047 Superose 6 5/150
1.43
30.0
25.0
20.0
15.0
10.0
5.0
0.0
UV280 (mAU)
A1 A2 A3 A4 A5 A6 A7 A8 A9 A10 A11 A12 B12
0.0
0.5
1.0
1.5
2.0
Elution volume (mL)

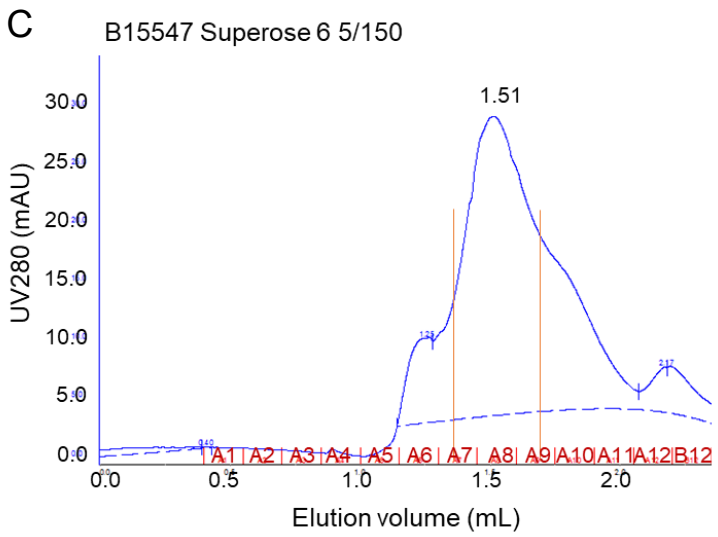
C
B15547 Superose 6 5/150
1.51
UV280 (mAU)
30.0
25.0
20.0
15.0
10.0
5.0
0.0
A1 A2 A3 A4 A5 A6 A7 A8 A9 A10 A11 A12 B12
0.0
0.5
1.0
1.5
2.0
Elution volume (mL)

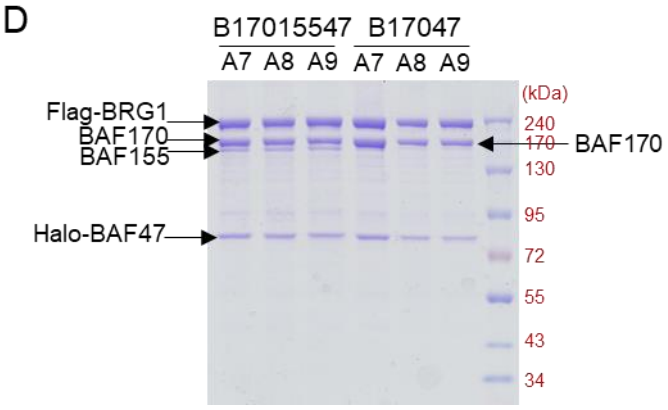
D
B17015547 B17047
A7 A8 A9 A7 A8 A9
(kDa)
Flag-BRG1
BAF170
BAF155
Halo-BAF47
240
170
130
95
72
55
43
34
BAF170

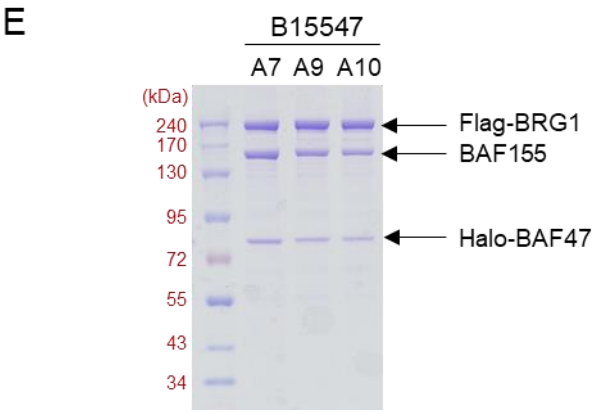
E
B15547
A7 A9 A10
(kDa)
240
170
130
95
72
55
43
34
Flag-BRG1
BAF155
Halo-BAF47

Figure 12. The SEC results from Superose 6 5/150 column indicated that peaks of the complexes BRG1+BAF170+BAF155+BAF47 (shorted as B17015547), BRG1+BAF170+BAF47 (shorted as B17047), BRG1+BAF155+BAF47 (shorted as B15547) were at the nearly same position of elution volume.

A, B and C, Protein were purified with anti-Flag M2-agarose beads. Protein samples were subjected to Superose 6 5/150 size exclusion column and results were shown. D and E, The peak fractions were analyzed with SDS-PAGE and gels were stained with coomassie brilliant blue.

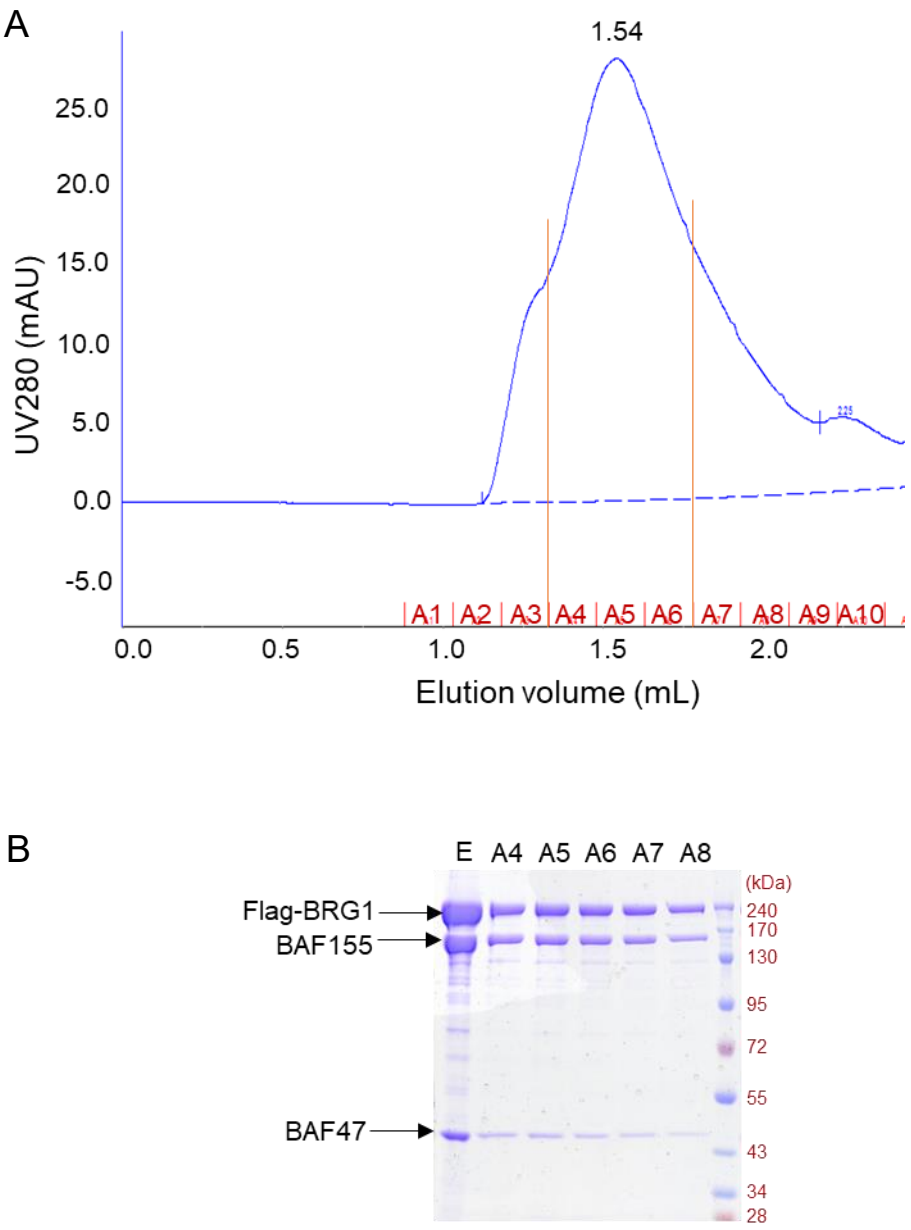

Figure 13. The complex was formed by Flag-BRG1, BAF155 and BAF47.

A, Sf9 cells were co-infected with baculoviruses for expressing Flag-tagged BRG1, untagged BAF155 and BAF47. Cells were harvested 72 hours post-infection. Cell lysate was incubated with anti-Flag M2-agarose beads. Protein sample eluted from beads was subjected to Superose 6 5/150 size exclusion column and result was shown. B, Elution and peak fractions were analyzed with SDS-PAGE and gel was stained with coomassie brilliant blue. 'E' indicated elution from M2 beads.

2.3.2 BRG1, BAF155 and BAF47 formed stable core SWI/SNF complex

To prepare the sample for EM in the following, 1 liter of Sf9 cells were co-infected with baculovirus for expressing Flag-tagged BRG1, and baculovirus for expressing untagged BAF155 and BAF47. After 72 hours post-infection, cells were harvested and lysed by nuclear extraction method to achieve Flag-BRG1 + BAF155 + BAF47 complex by incubating with anti-Flag M2-agrose beads. The protein sample eluted from M2-agrose beads was concentrated to 500 µL and loaded to Superose 6 10/300 GL size exclusion column with a bed volume of 24 mL, which separated and purified protein efficiently. The size exclusion chromatography result showed a sharp and symmetric peak (**Figure 14**), indicating that the protein sample was homogenous. Then the central peak fractions were collected for next steps. Approximately 300 µg protein yield was achieved from 1 liter of Sf9 cells.

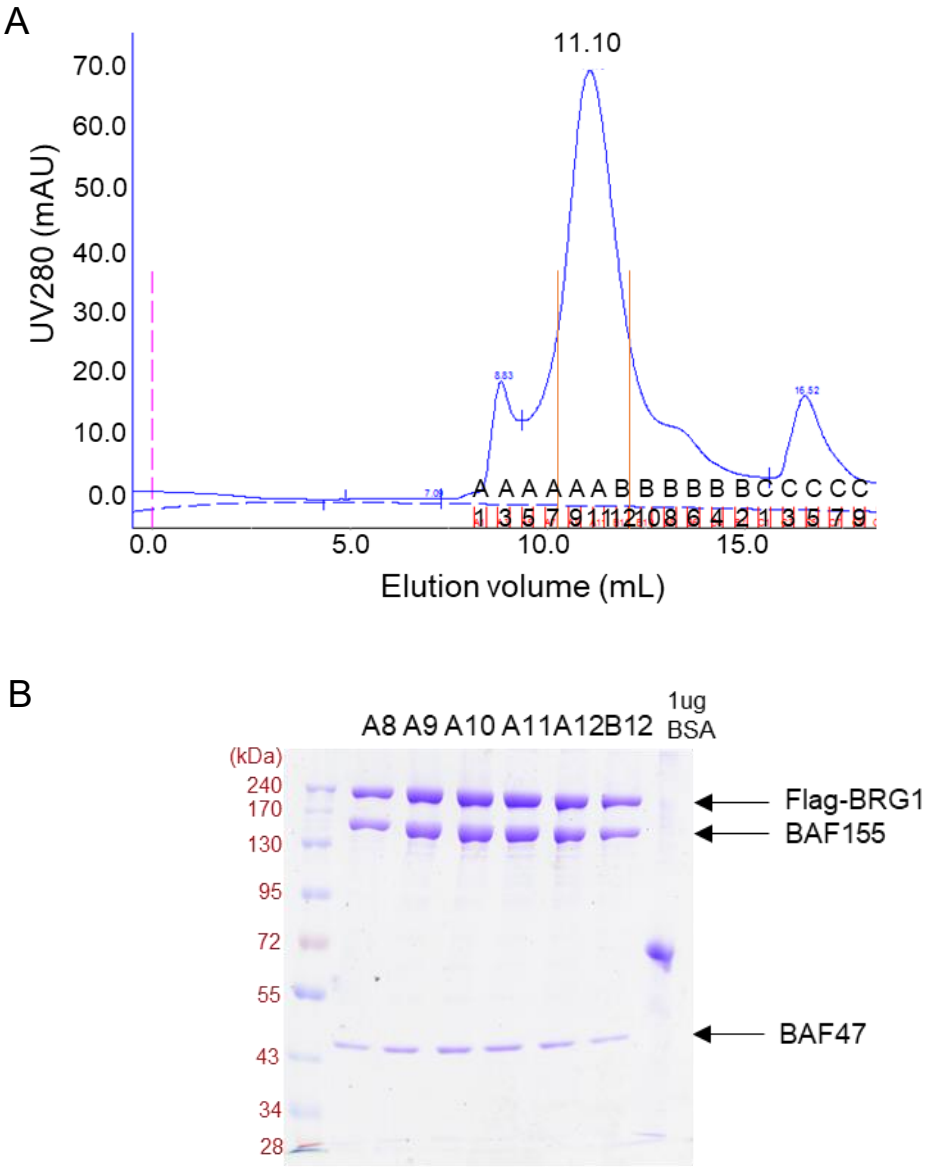

Figure 14. The purification of core SWI/SNF complex composed of BRG1, BAF155 and BAF47.

A, Protein sample was subjected to Superose 6 10/300 size exclusion column and results were shown. B, 6 μL of sample from each peak fraction of 300 μL were analyzed with SDS-PAGE and gel was stained with coomassie brilliant blue. 1 μg of BSA was loaded on gel to estimate protein yield.

2.3.3 The core SWI/SNF complex bound to nucleosome effectively

To check the biochemical activity of recombinant core SWI/SNF complex, the nucleosome binding ability of core SWI/SNF complex was assessed through electrophoretic mobility shift assay (EMSA). EMSA result showed that free nucleosome core particles (NCPs) decreased with increasing amount of SWI/SNF complex (**Figure 15**), indicating that the recombinant core SWI/SNF complex had the ability of binding to nucleosome. The NCPs bound with core SWI/SNF complex could not be shown in the gel, because the SWI/SNF-NCP complex was too big to run into the 4.0% native TBE polyacrylamide gel. Thus, the amount of bound NCPs was assessed by free NCPs relative to total amount of NCPs.

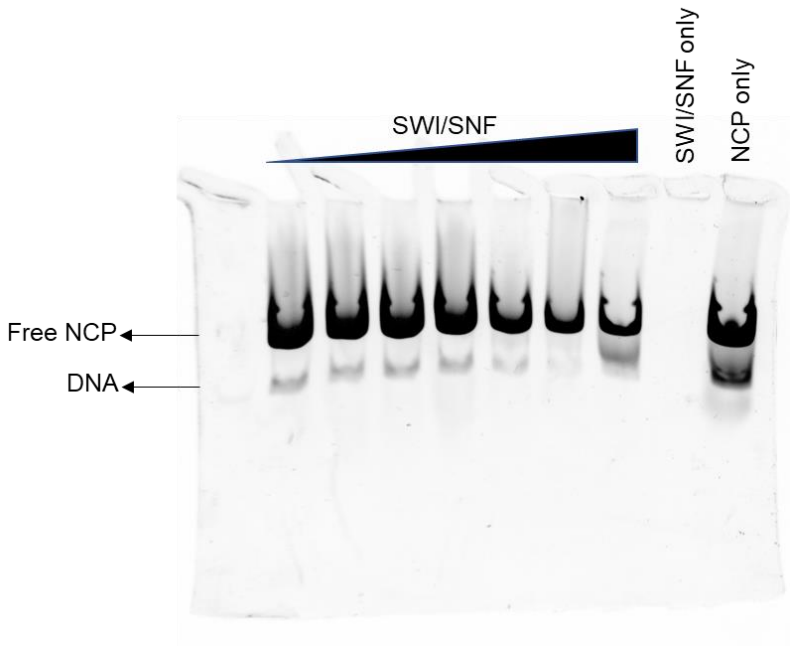

Figure 15. EMSA result indicated that the recombinant core SWI/SNF complex had the ability of binding to nucleosome.

20 μM nucleosome was incubated with increasing amount of SWI/SNF from 1 μM to 20 μM, 3 mM ADP, 3 mM BeSO4, 10 mM NaF and 10 mM $MgCl_2$. After incubation on ice for 30 min, the samples were resolved by electrophoresis on 4.0% native TBE polyacrylamide gels at 70 V for 90 min at 4 ℃. The gels were stained with SYBR Gold nucleic acid gel stain and imaged. The lower band was electrophoresis-caused DNA fragments dissociated from NCPs. The upper band was free NCPs unbound by SWI/SNF complex.

2.3.4 Grafix stabilized core SWI/SNF complex for negative staining EM

The best fractions from size exclusion chromatography were collected and applied to negative staining EM to check the protein particle quality. However, the result showed that most of the complex particle dissociated under negative staining EM (**Figure 16**). To make the sample stable for EM, sample was stabilized by the method of GraFix as described in Materials and Methods. After sample was stabilized, it only showed one band with the molecular weight of the complex in SDS-PAGE (**Figure 17**). This was because the covalent bond formed within protein complex and cross-linking agent glutaraldehyde after cross-linking could not be broken by SDS (sodium dodecyl sulfate) and high temperature denaturation. Then central peak fractions, including fraction 10 (F10) and fraction 11 (F10), with core SWI/SNF complex were checked by negative staining EM. The results showed that the sample quality was much improved with less complex dissociation and improved homogeneity after GraFix cross-linking and purification (**Figure 18**). Finally, the central peak fractions were pooled, and then concentrated to the concentration of 500 ng/μL for cryo-EM sample preparation.

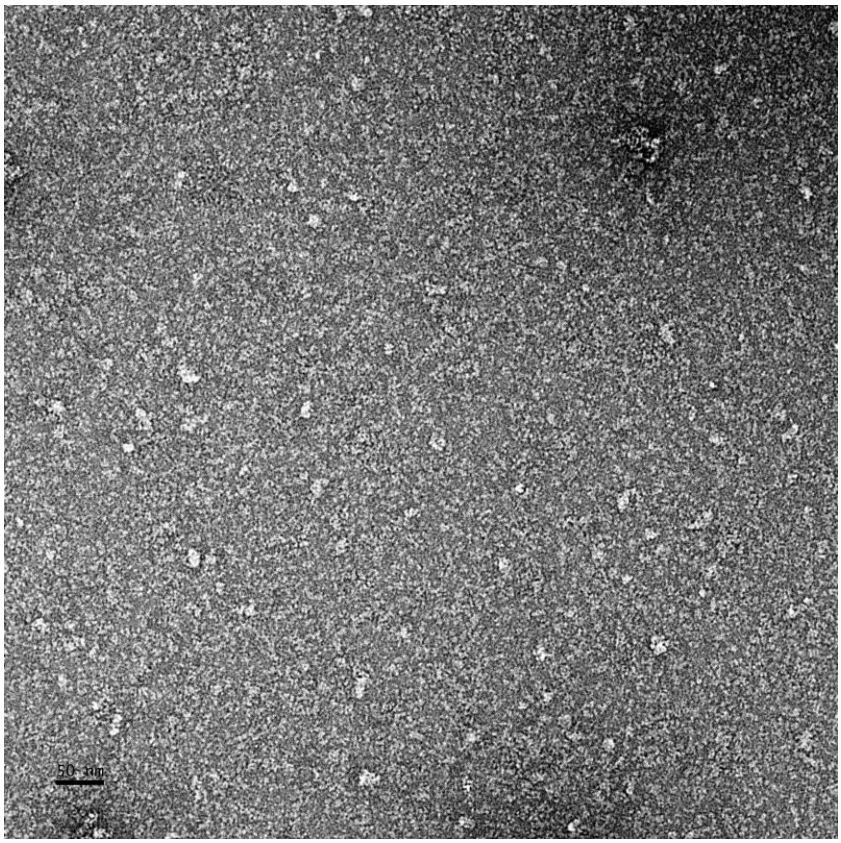

Figure 16. The negative staining result of native core SWI/SNF complex.

3 μL of core SWI/SNF complex sample with the concentration of 100 ng/μL was pipetted on the glow-discharged holey grid and stained with 0.75% uranyl formate (UF). The grid was observed using a 120 kV Tecnai F20 microscope (FEI) at a magnification of ×49,000. Scale bar = 50 nm.

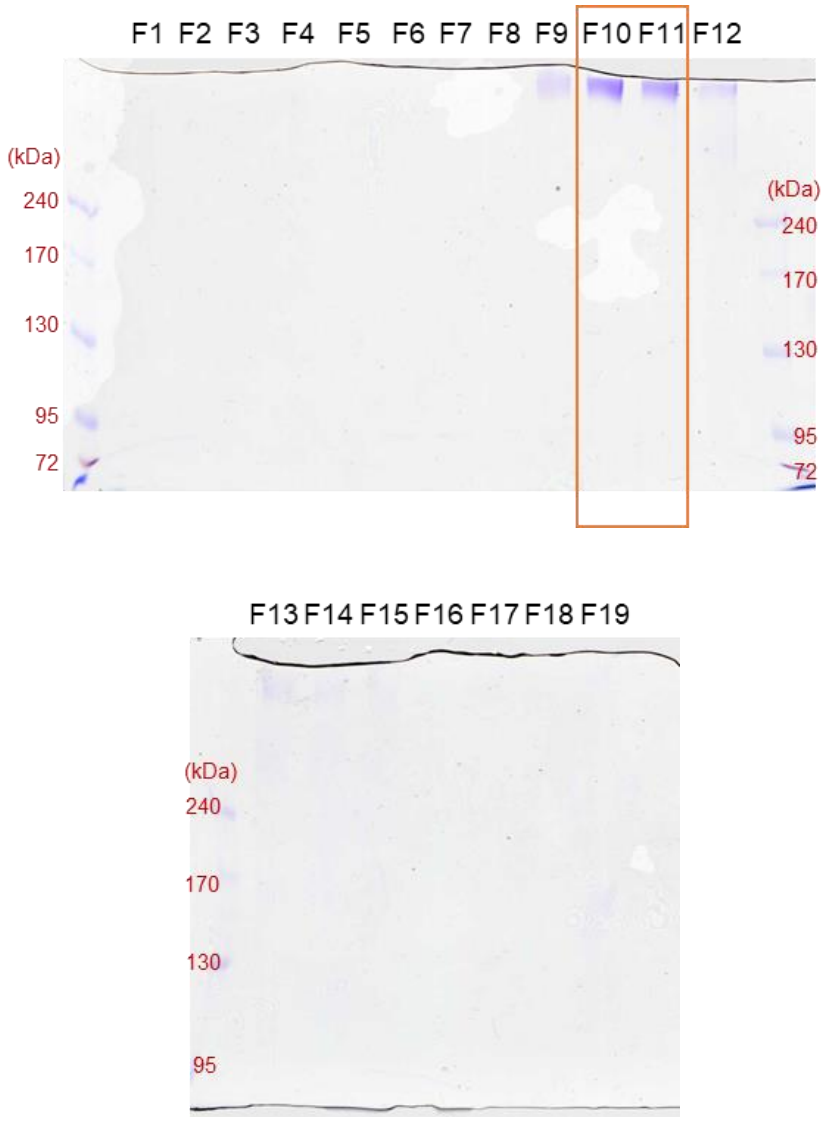

Figure 17. Fractions of core SWI/SNF complex after GraFix ultracentrifugation were collected and analyzed.

After GraFix ultracentrifugation, the gradients were fractionated from bottom to top (from FI to F19) and analyzed with 6% SDS-PAGE gels. The gels were stained with coomassie brilliant blue. F10 and F11 were the best fractions with sample of core SWI/SNF complex.

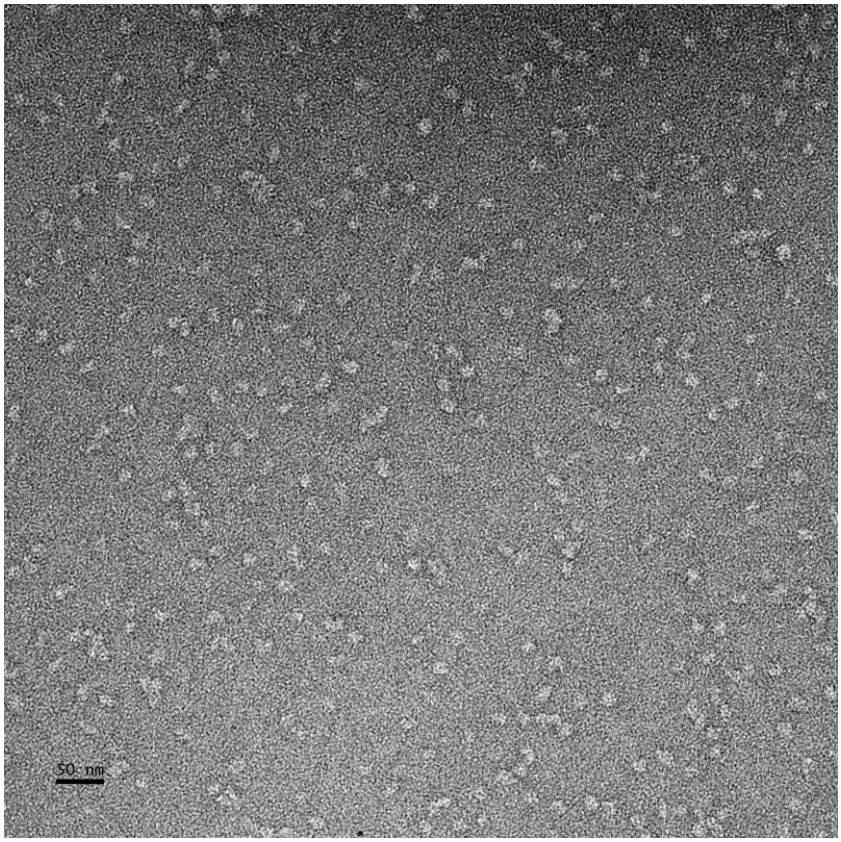

Figure 18. The negative staining result of core SWI/SNF complex after GraFix.

3 µL of GraFix-stabilized core SWI/SNF complex sample with the concentration of 100 ng/µL was pipetted on the glow-discharged holey grids and stained with 0.75% UF. The grid was observed using a 120 kV Tecnai F20 microscope (FEI) at a magnification of ×49,000. Scale bar = 50 nm.

2.3.5 Preliminary cryo-EM result of core SWI/SNF complex

To prepare cryo-EM grid, 4 µL of sample with concentration of 500 ng/µL was pipetted on C-flat holey carbon grid and applied for plunge freezing with the condition of 5.5 second blot time and -23 blot force. The EM grid screening results indicated that the blot condition made suitable thickness of ice for EM imaging. Moreover, no ice contamination appeared on the grids. However, the sample concentration was not high enough so that the particle number was not enough for further data processing. More proteins would be purified to rich higher concentration for EM. In addition, some particle aggregations appeared in EM micrograph (**Figure 19**), thus, the buffer conditions of sample need to be optimized to get homogeneous and monodisperse single particles for further data collection and processing, such as adding arginine, reducing agent or detergent.

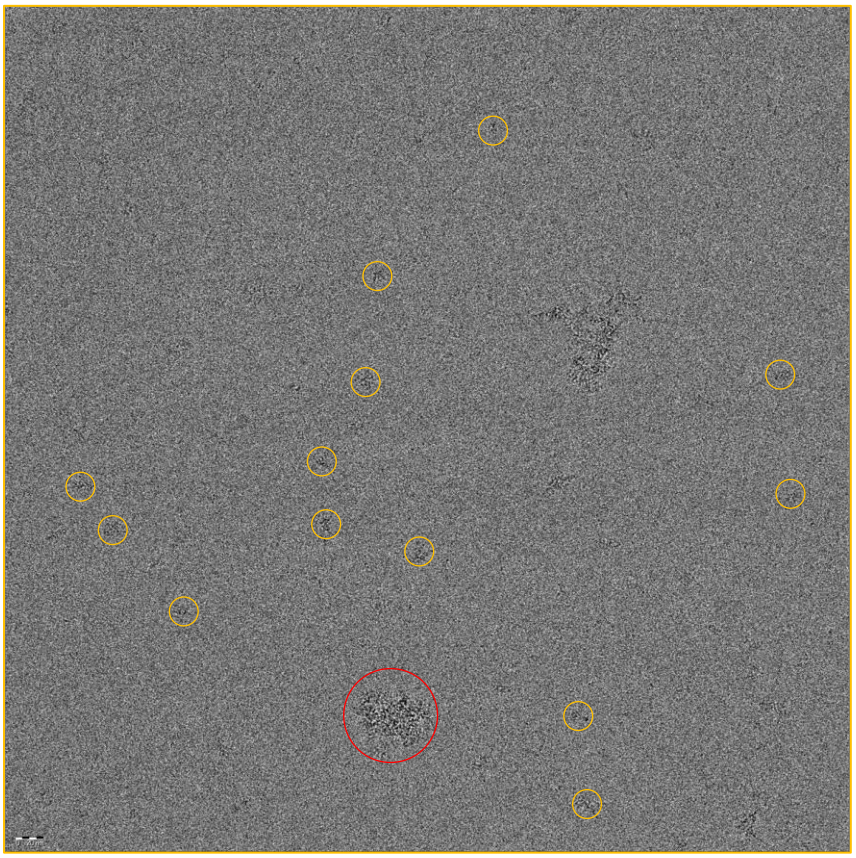

Figure 19. The preliminary cryo-EM result of core SWI/SNF complex (Data collected by Bob Ashley).

4 µL core SWI/SNF complex sample with the concentration of 500 ng/µL was applied to a glow-discharged Quantifoil holey carbon grid. The grid was applied to plunged freezing and observed using a Titan Krios microscope (FEI) operated at 300kV, equipped with a Gatan K2 Summit camera. Single-particles were circled in yellow and aggregates was circled in red. Scale bar = 50 nm.

2.4 Discussion and future directions

In Chapter 2, the core SWI/SNF complex composed of BRG1, BAF155, and BAF47 was purified from Sf9 insect cells infected with baculoviruses. Protein sample was loaded onto Superose 6 10/300 size exclusion column for homogenizing and purification. The negative staining EM result of native complex showed dissociation of protein complexes. So, the method of GraFix was applied to stabilize protein complex and the negative staining EM showed that the fixed sample had much improved stability and homogeneity. Finally, the sample was subjected to cryo-EM for imaging. The result showed that the blot conditions of preparing sample grids were suitable for optimal ice thickness and protein particles were shown on grids under EM. However, the density of single particles was not enough for further data processing and protein aggregates appeared on grid. Thus, the buffer condition for optimal particle distribution is needed to be optimized in future work.

The first part of future works contains data collection and data processing for structure determination. The sample of core SWI/SNF complex will be optimized for cryo-EM imaging, data collection and data processing. In data processing, a few micrographs are used to select suitable particles manually, typically around a thousand particles. The particles are subjected to a 2D classification, at least 50-100 particles contributing on average to each class. From the resulting 2D classifications, a few (usually not more than 5-10) representative views are selected as template for automated particle picking of all micrographs. The auto-picked particles are subject to 2D classification and 3D classification

based on initial model to select suitable particles for high-resolution structure determination. The selected particles are divided into several subsets based on the representative conformations. Particle polishing and 3D auto-refinement are applied resulting in the 3D reconstructions at near-atomic resolution (around 4.0 Å). Then, the structural model is built by fitting the crystal structures to the EM density map. Computational methods for fitting atomic structures into cryo-EM maps bridge the resolution gap between cryo-EM and X-ray crystallography, allowing for interpretation of cryo-EM data beyond the nominal resolution. The structures are superimposed using the sequence alignment and the fits are refined by iteratively removing bad residue pairings. Many modeling methods for cryo-EM maps have been developed, such as rigid domain fitting, homology modeling, and de novo modeling [66]. Finally, the accurate and detailed 3D models of intricate biological structures is achieved. Based on the structural information, the model of chromatin remodeling mechanism is schematically illustrated. To identify the conformational change of nucleosome by remodeling, the structures of free NCP and SWI/SNF-NCP complex are compared to figure out the structural differences.

The second part of future works is to identify the interface within core SWI/SNF complex and nucleosome based on structural information, and make mutations of residues on the interface to confirm the structure through some biochemical activity assays. Because the reaction of chromatin remodeling is ATP-dependent and BRG1 is the ATPase subunit in the SWI/SNF complex, ATPase activity of core SWI/SNF complex could be measured. If some mutations of the residues within the interface of core SWI/SNF complex caused reduction of

ATPase activity, it would indicate that these residues were critical for regulating ATPase activity of BRG1. Moreover, the chromatin remodeling activity of SWI/SNF could be measured with the restriction-enzyme accessibility assay. This assay is based on the theory that the positioned histone octamer shields a restriction enzyme recognition site (we will use HhaI, whose cleavage site is GCGC) which can be exposed by ATP-dependent nucleosome remodeling to allow DNA cleavage, as shown in **Figure 20**. If some mutations of the residues within the interface of core SWI/SNF complex caused decreasing of chromatin remodeling activity, it would indicate that these residues were critical for regulating chromatin remodeling activity of the complex. In summary, these biochemical activity assay together with structural information would illustrate the mechanism of core SWI/SNF complex on nucleosome remodeling.

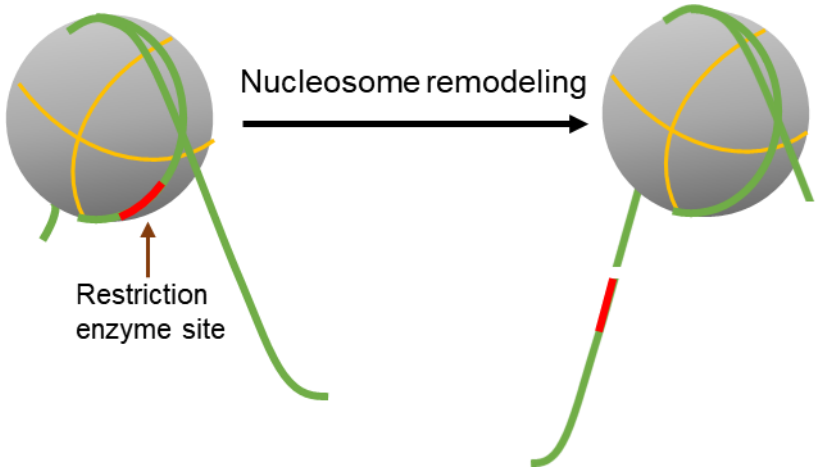

Figure 20. Restriction-enzyme accessibility assay (Derived from www.epicypher.com). The restriction enzyme site is included in the DNA fragment of nucleosome. Originally the restriction enzyme site is shielded by histone octamer and inaccessible to restriction enzyme (Left). After nucleosome remodeling, the enzyme site is exposed and accessible to restriction enzyme, so that the DNA is cleaved (Right).

Chapter 3 Nucleosome reconstitution

3.1 Introduction

As the basic repeating subunit of chromatin, the nucleosome is formed by the tight association between histones and DNA to protect genetic information from nuclease digestion [67]. Nucleosome can be obtained by two ways, purification from in vivo natural sources or reconstitution from in vitro recombinant histones and nucleosome positioning DNA. The reconstituted nucleosome has the benefits over purified from nature sources, because recombinant nucleosome contains no posttranslational modifications and can be obtained in high purity and high expression levels, so that reconstituted nucleosomes are more compositionally uniform to improve homogeneity.

The developed method of expressing histone proteins in bacteria has allowed the structural determination of nucleosome core particles (NCPs) at high resolution [67]. As shown in **Figure 21**, the structure of nucleosome contains a DNA fragment and a histone octamer assembled by two copies of each histone proteins H2A, H2B, H3 and H4. The DNA fragment wraps around histone octamer to form a disc-like structure with a height of 5.5 nm and a diameter of 11 nm. The histone dimers associate with each other primarily via helix bundles at the dimer-dimer interfaces by the formation of H2A-H2B:H4-H3:H3-H4:H2B-H2A. The H3/H4 dimer self-associates via an H3:H3 interface to form a stable tetramer. A single H2A/H2B dimer associates with either end of the H4/H3:H3/H4 tetramer via a H4:H2B helix bundle. The DNA binding sites are arranged along the outer edge of histones.

In this chapter, we aimed to reconstitute nucleosomes for researching the chromatin remodeling mechanism of SWI/SNF complex. We reconstituted nucleosomes in vitro by wrapping DNA fragments around the recombinant histone octamers and acquired the electron density map of nucleosome by cryo-EM imaging and data processing. The crystal structure of nucleosome was fitted into EM density map, which proved our reconstituted nucleosome to be valid.

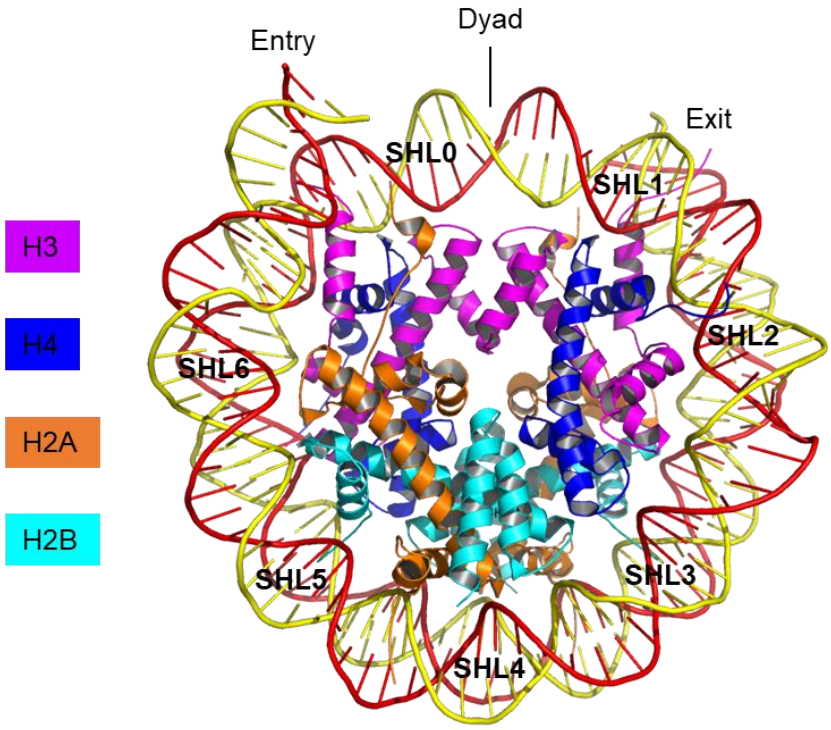

Figure 21. Structure of nucleosome (Derived from PDB: 5X0Y, Snf2 was omitted from the structure).

The structure shown is a view looking down the DNA superhelix axis. Superhelix sites are indicated with numbers, from SHL0 to SHL6. Histone proteins and DNA strands are indicated with different colors. Histone H3, magenta; H4, blue; H2A, orange; H2B, cyan; 5'-DNA, yellow; 3'-DNA, red.

3.2 Materials and Methods

3.2.1 The expression and purification of histone proteins

The *Xenopus laevis* histone genes for H2A, H2B, H3 and H4 were cloned into pET vectors (pET3a or pET3d) without tag in T7 expression system, as described previously [68]. Then the pET-histone expression plasmids were transfected into BL21 (DE3) *E.coli* cells. The cells were cultured and shaken in Terrific Broth (TB) medium at 37 ℃. When OD_{600} reached to 0.6-0.8, Isopropyl-β-D-1-thiogalactopyranoside (IPTG) was added to cultured cells to a final concentration of 0.5 mM. The time after IPTG induction for expression was 4-5 hours at 37 ℃. Cells were harvested by centrifugation. Cells pellet was resuspended with lysis buffer [50 mM HEPES, 150 mM NaCl, pH 7.8, 1 mM EDTA, 1% Triton X-100, 1 mM PMSF (protease inhibitor)], and sonicated to lysed cells. Then cell lysate was centrifuged at 12,000 rpm for 30 min and pellet containing inclusion bodies was collected for histone purification. Inclusion bodies were washed with lysis buffer for three times to remove cell debris. Then inclusion bodies were resuspended and dissolved with unfolding buffer [20 mM HEPES, 6 M guanidinium hydrochloride, pH 7.8, 10 mM DTT] and stir gently for 1-2 hours at room temperature. The undissolved material was removed by centrifugation. The supernatant was collected and dialyzed against low salt buffer [20 mM sodium acetate, 7 M urea, 200 mM NaCl, pH 5.2, 1 mM EDTA, 2 mM DTT]. Then sample was applied to HiTrap SP HP cation exchange chromatography column, which has been equilibrated with low salt buffer [20 mM sodium acetate, 7 M urea, 200 mM NaCl, pH 5.2, 1 mM EDTA, 2 mM DTT]. Then histone proteins were eluted from column

with high salt buffer [20 mM sodium acetate, 7 M urea, 2 M NaCl, pH 5.2, 1 mM EDTA, 2 mM DTT]. The peak fractions were analyzed with SDS-PAGE. Fractions containing histone proteins were pooled. The molarity of each histone was calculated.

3.2.2 Assembly of histone proteins into octamer

Histone proteins were combined with equal molarity and placed into a 6-8 kDa dialysis bag and dialyzed against refolding buffer [20 mM HEPES, 2 M NaCl, pH 7.5, 2 mM EDTA, 2 mM DTT] at 4 ℃ for 18 hours, in which refolding buffer was changed every 6 hours. The high salt in refolding buffer can block the charges of histone protein, decreasing repelling force between histones, resulting in refolding. After dialysis, precipitate in sample was removed by centrifugation. Protein sample was concentrated and loaded onto Superdex 200 size exclusion chromatography column. Peak fractions were analyzed by SDS-PAGE and fractions with pure octamer were pooled.

3.2.3 Reconstitution of nucleosome core particle from DNA and octamer

Nucleosome reconstitution required histone octamer and DNA to be combined. The designed nucleosomal DNA fragment contained a '601' positioning sequence, an extranucleosomal linker DNA (50-bp) at one end and no linker DNA at the other end. The '601' positioning sequence has been reported to have high binding affinity to histone octamer and have a correspondingly strong nucleosome positioning ability [69]. The '601' positioning sequence is (5′-strand:

TCAGGATGTATATATCTGACACGTGCCTGGAGACTAGGGAGTAATCCCCTT GGCGGTTAAAACGCGGGGGACAGCGCGTACGTGCGTTTAAGCGGTGCTAG AGCTGTCTACGACCAATTGAGCGGCCTCGGCCCGGGATTCTCGAT) [69]. DNA fragments were inserted into pUC19 vector through the way of tandem repeating [70]. The plasmids were amplified and isolated from *E.coli*. The nucleosomal DNA fragments were released from plasmids by endonuclease digestion. DNA was purified with Mono Q anion exchanger and DEAE-5PW weak anion exchanger. Purified DNA and histone octamer were mixed with molarity ratio of 1:0.9 in high salt buffer [20 mM HEPES, 2 M NaCl, pH 7.5, 1 mM EDTA, 1 mM DTT] and dialyzed into buffers with decreasing salt to 250 mM NaCl. A gradual decreasing ionic force ensured proper nucleosome reconstitution. Finally, reconstituted nucleosome was purified with DEAE-5PW weak anion exchanger to remove unbound DNA with low salt buffer containing 250 mM NaCl and relatively high salt buffer containing 600 mM NaCl. Finally, nucleosome sample was loaded onto Superose 6 SEC column equilibrated with buffer [20 mM HEPES, 60 mM NaCl, pH 7.8, 1 mM EDTA, 1 mM DTT] to improve purity.

3.2.4 EM data collection and processing

The nucleosome sample was subjected to negative staining EM as describe above. The images were taken at a magnification of ×68,000. For cryo-EM, sample was applied to glow-discharged quantifoil holey carbon grid and grid was subjected to plunge freezing as described above. Sample was observed with electron microscope and imaged. EMAN2 software was used for data processing.

3.3 Results

3.3.1 Histone proteins H2A, H2B, H3 and H4 were purified

Histone proteins H2A, H2B, H3 and H4 were insoluble upon expression and accumulated in inclusion bodies. Purification of histones was performed by solubilizing inclusion bodies with guanidinium hydrochloride and subsequent ion exchange chromatography in the presence of urea. Urea can also dissolve histone proteins but its ability to dissolve insoluble proteins is weaker than guanidinium hydrochloride. However, guanidinium hydrochloride is damaged to the sepharose column whereas urea is not. Histone proteins were purified with HiTrap SP HP cation exchange chromatography column because of their positive charges (**Figure 22A, B, C and D**). The SDS-PAGE result showed that the purified histones had the molecular weight (**Figure 22E**) consistent with as expected in **Table 4**. Moreover, the yields of H2A, H2B and H3 were typically 50-80 mg of pure protein per liter of cultured bacteria, whereas the yield of H4 was much lower, typically 10 mg of pure protein per liter of cultured bacteria, probably because of the degradation by protease. Thus, more cells were needed for histone H4 purification to reach the amount for following assembly with other histones.

A

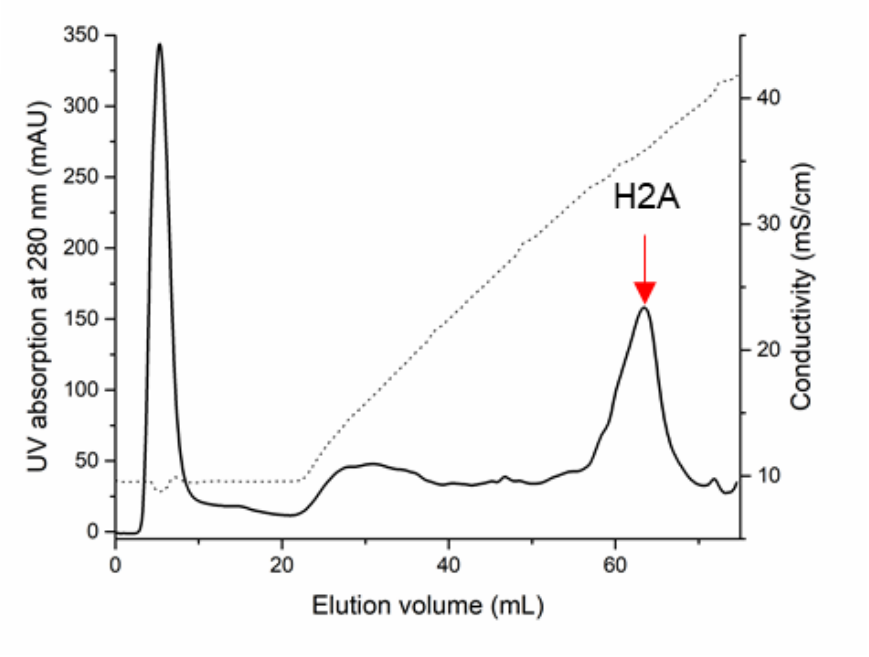
UV absorption at 280 nm (mAU)
Conductivity (mS/cm)
Elution volume (mL)
H2A
350
300
250
200
150
100
50
0
40
30
20
10
0
20
40
60

B

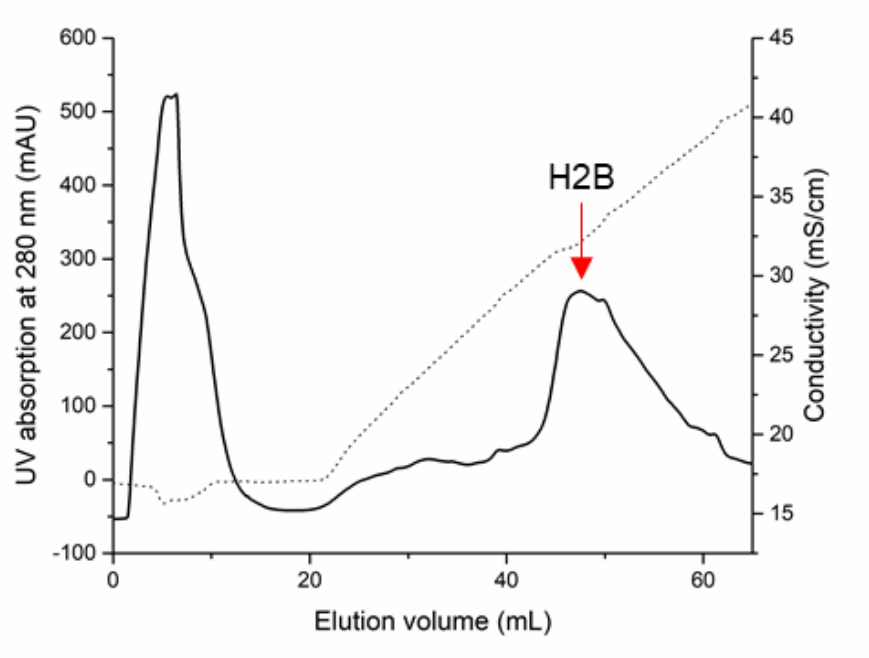
UV absorption at 280 nm (mAU)
Conductivity (mS/cm)
Elution volume (mL)
H2B
600
500
400
300
200
100
0
-100
45
40
35
30
25
20
15
0
20
40
60

C

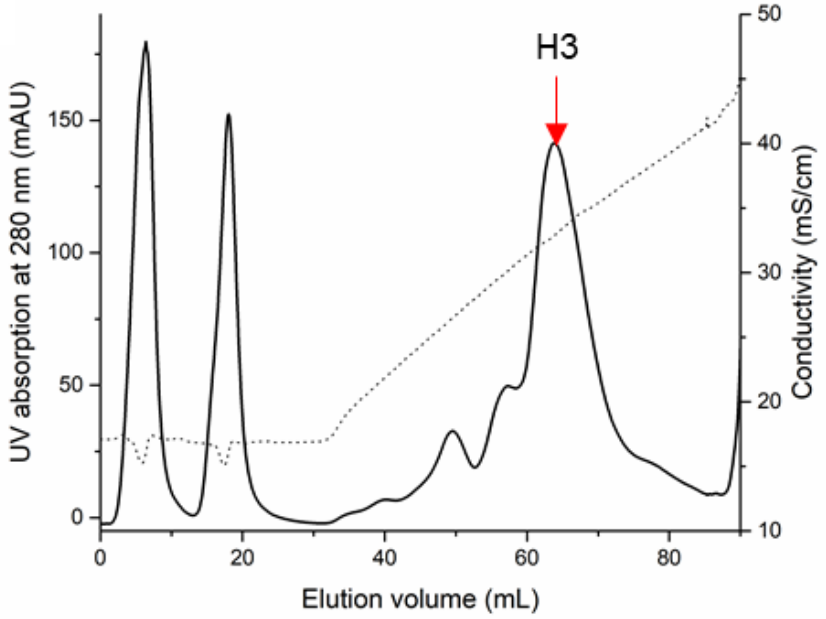
H3
UV absorption at 280 nm (mAU)
Conductivity (mS/cm)
Elution volume (mL)
0
50
100
150
10
20
30
40
0
20
40
60
80

D

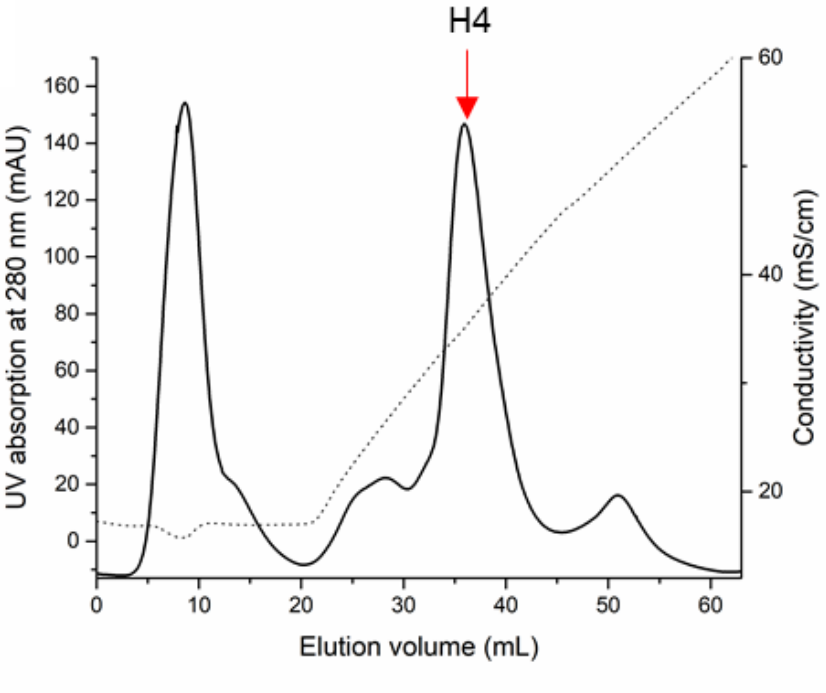
H4
UV absorption at 280 nm (mAU)
Conductivity (mS/cm)
Elution volume (mL)
0
20
40
60
80
100
120
140
160
20
40
60
0
10
20
30
40
50
60

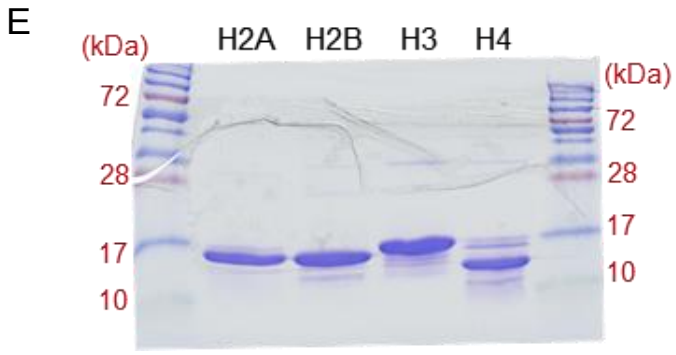

Figure 22. Histone proteins H2A, H2B, H3 and H4 were purified (Completed by collaboration with Dr. Junsheng Zhu).

A, B, C and D, Histone proteins H2A, H2B, H3 and H4 were purified with HiTrap SP HP cation exchange chromatography column, respectively. E, Histone samples after purification were analyzed with SDS-PAGE and gel was stained with coomassie brilliant blue.

Table 4. Molecular weight of histone proteins (Derived from [71]).

Histone	Molecular weight (Dalton)
H2A	13,960
H2B	13,774
H3	15,273
H4	11,236

3.3.2 Histone proteins H2A, H2B, H3 and H4 were refolded to form histone octamer

The entire histone octamer is formed only when wrapped around by DNA or in solutions of high salt (~2M) due to the high positive charge of the component proteins. The high salt shields the positive charge of histone components so that components refold to form octamer because of the hydrophobic effect. To improve purity, H2A and H2B were combined to form H2A/H2B dimer; H3 and H4 were combined to form H4/H3:H3/H4 tetramer; then H2A/H2B dimer and H4/H3:H3/H4 tetramer were combined to form octamer. The separation of histone octamer from H4/H3:H3/H4 tetramer with size exclusion chromatography was not complete because the peaks of octamer and H4/H3:H3/H4 tetramer had a big overlap (**Figure 23A**), whereas H2A/H2B dimer can be separated from octamer. Thus, excess H2A/H2B dimer was used to make sure all H4/H3:H3/H4 tetramer were combined with H2A/H2B dimer. After each step of refolding for combination, sample was subjected to Superdex 200 size exclusion chromatography column for purification. The peak of octamer was sharp and symmetric, indicating the high purity of octamer (**Figure 23A**). The SDS-PAGE results also showed high purity of H2A/H2B dimer, H4/H3:H3/H4 tetramer, and octamer (**Figure 23B**).

A

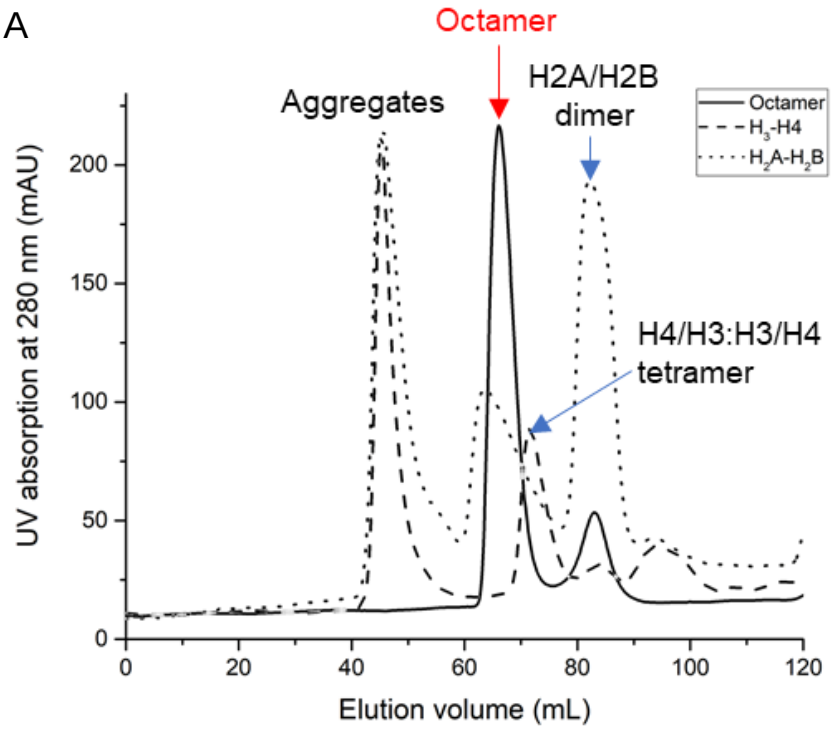
Octamer
H2A/H2B
dimer
Aggregates
Octamer
H3-H4
H2A-H2B
H4/H3:H3/H4
tetramer
UV absorption at 280 nm (mAU)
Elution volume (mL)
0
50
100
150
200
0
20
40
60
80
100
120

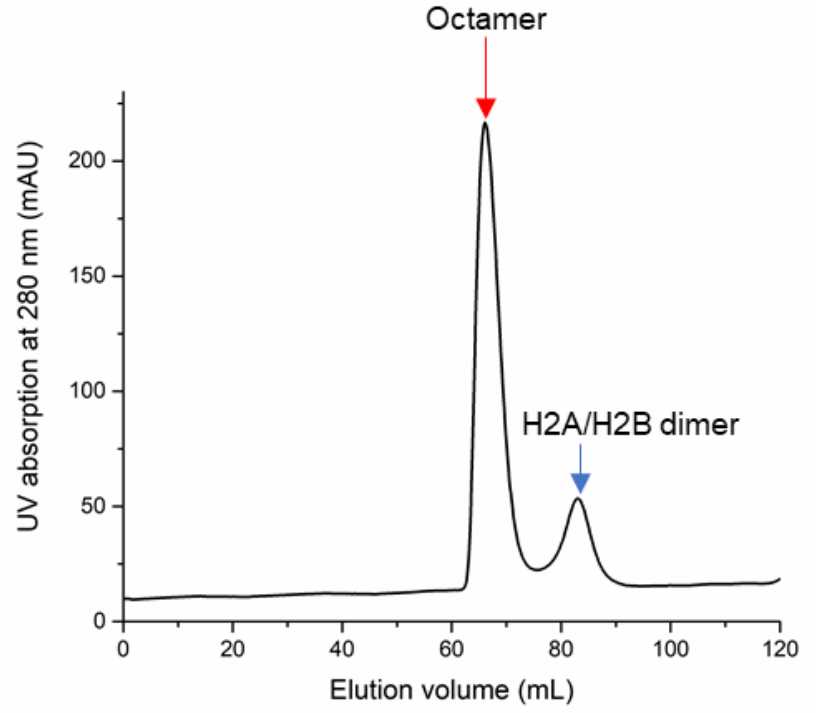
Octamer
H2A/H2B dimer
UV absorption at 280 nm (mAU)
Elution volume (mL)
0
50
100
150
200
0
20
40
60
80
100
120

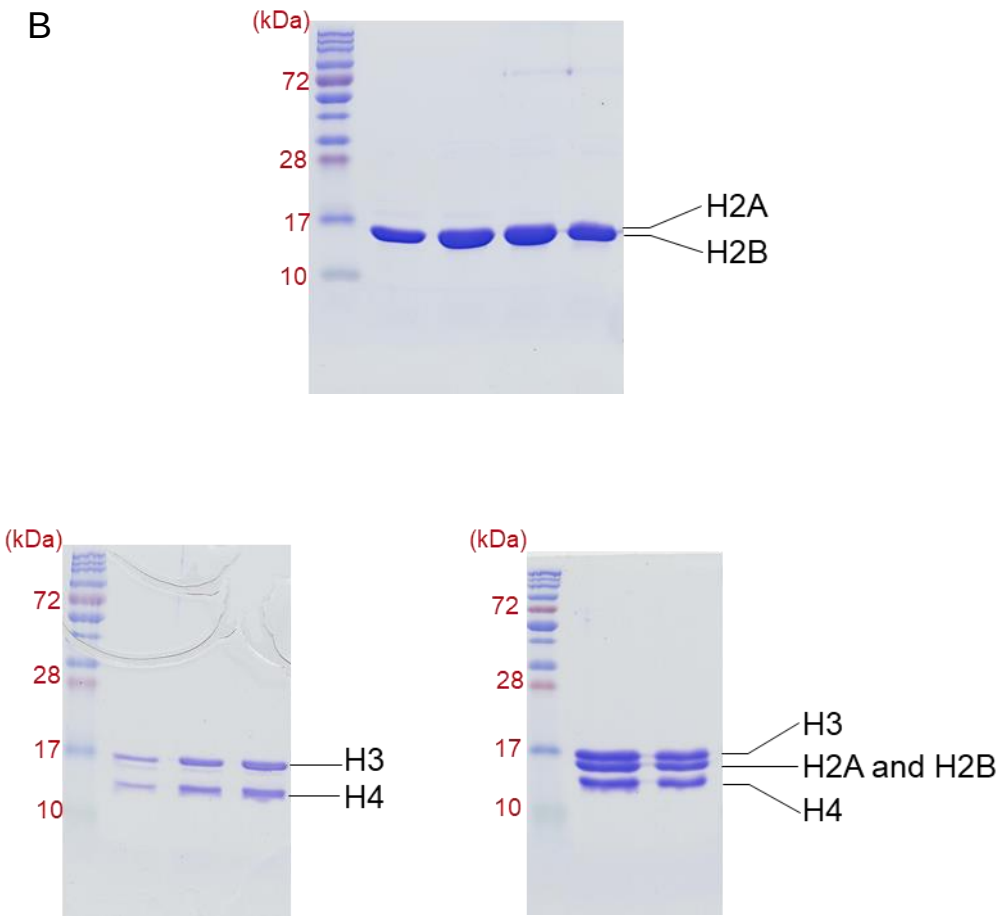

Figure 23. Histone proteins H2A, H2B, H3 and H4 were refolded to form histone octamer (Completed by collaboration with Dr. Junsheng Zhu).

A, H2A and H2B were combined to form H2A/H2B dimer; H3 and H4 were combined to form H4/H3:H3/H4 tetramer; then H2A/H2B dimer and H4/H3:H3/H4 tetramer were combined to form octamer. Samples were loaded onto Superdex 200 size exclusion chromatography column at each step. B, Samples after purification were analyzed with SDS-PAGE and gels were stained with coomassie brilliant blue. Upper, H2A/H2B dimer; Left lower, H4/H3:H3/H4 tetramer; Right lower, Octamer.

3.3.3 DNA was purified and wrapped around histone octamer to form nucleosome core particle

The nucleosomal DNA fragment was designed to contain a '601' positioning sequence, an extranucleosomal linker DNA (50-bp) at one end and no linker DNA at the other end. The '601' positioning sequence was reported to have high binding affinity to histone octamer and have a correspondingly strong nucleosome positioning ability, so it has been commonly used for nucleosome reconstitution [69]. The plasmids inserted with the nucleosomal DNA fragments were amplified and isolated from *E.coli*. The DNA fragments were released from plasmids by endonuclease digestion and purified with Mono Q anion exchanger to remove cleaved vectors after digestion (**Figure 24A)**. The DNA sample was further purified with DEAE-5PW weak anion exchanger to improve purity (**Figure 24B**). The DNA fragments were purified with anion exchangers due to the negative charge. Then DNA was wrapped around histone octamer to form nucleosome. Nucleosomes formed spontaneously by mixing DNA and histone in high salt solutions and then gradual removal of the salt through the way of dialyzing against low-salt buffer gradually. In low-salt buffer, nucleosome formed with the ionic bond between octamer and DNA. Then nucleosomes were purified with DEAE-5PW weak anion exchanger to remove unbound free DNA (**Figure 24C**). Here, DEAE-5PW weak anion exchanger was used because low-salt buffer was enough to elute nucleosome from this column. This avoided the use of high-salt buffer because high salt would destroy nucleosome. In the last, nucleosomes were subjected to Superose 6 size exclusion chromatography column for further purification and the

peak was sharp and symmetric, indicating the high purity of nucleosomes (**Figure 24D**).

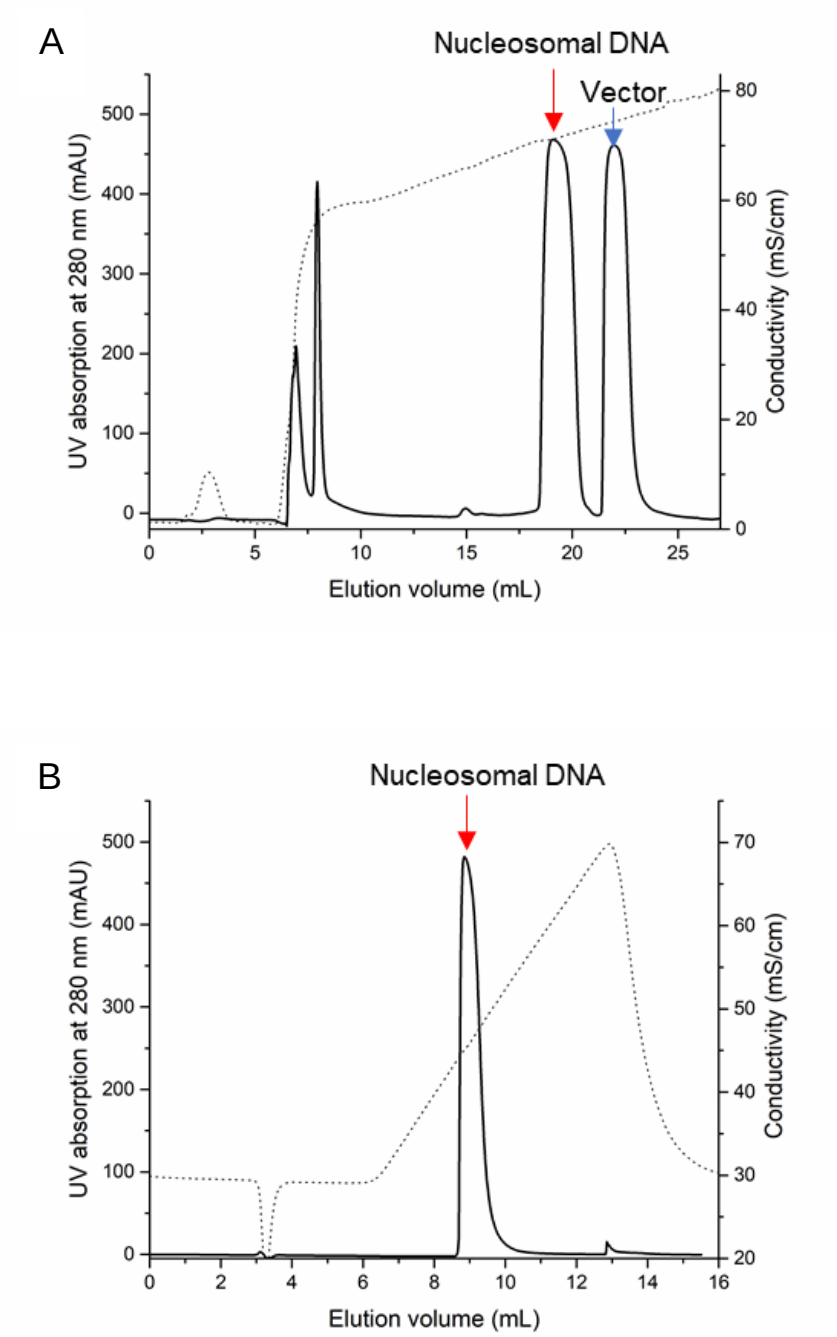

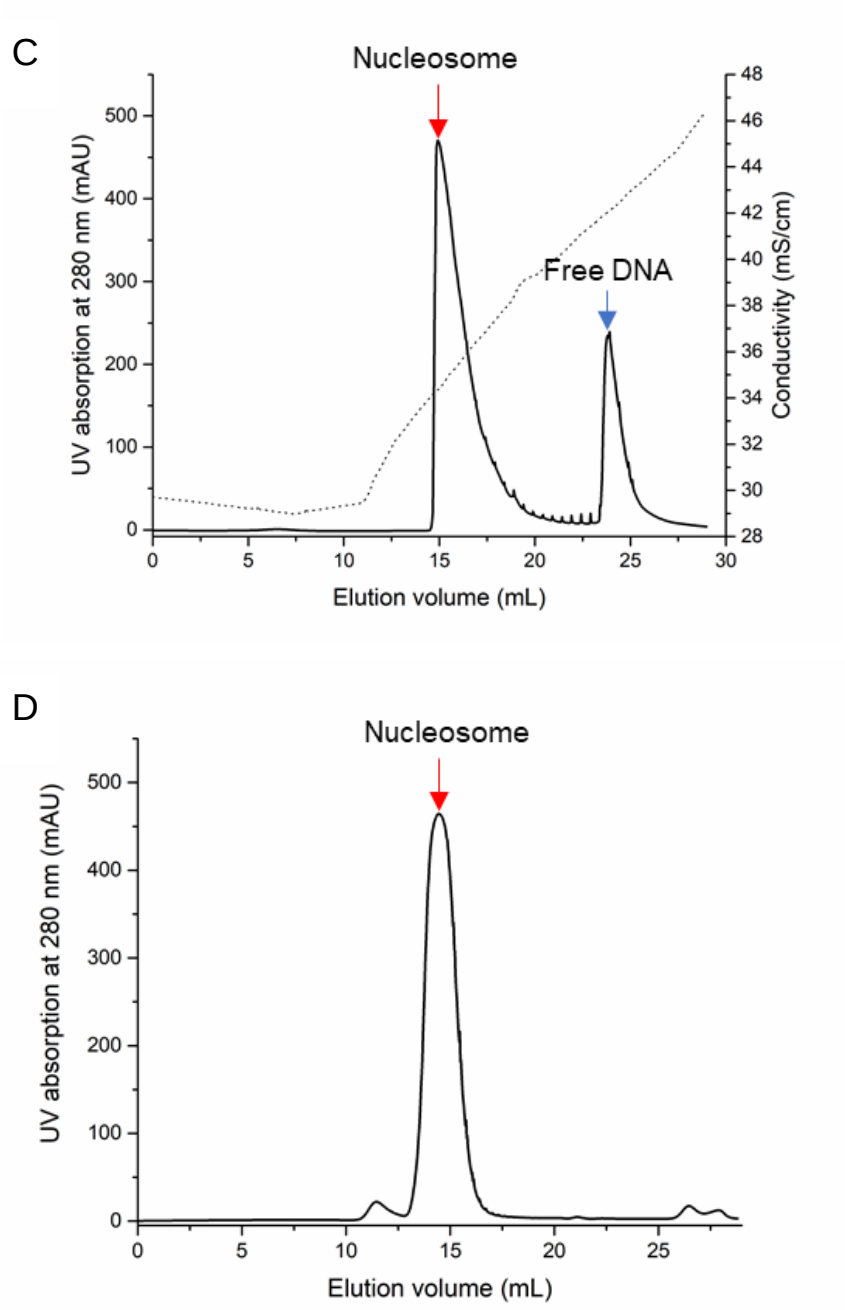

Figure 24. Nucleosomal DNA was purified and wrapped around histone octamer to form nucleosome core particle (Completed by collaboration with Dr. Junsheng Zhu). A, DNA was purified with Mono Q anion exchange chromatography to remove vectors after endonuclease digestion. B, DNA purified from (A) was furtherly purified with DEAE-5PW weak anion exchanger. C, Nucleosome was purified with DEAE-5PW weak anion exchanger to remove unbound free DNA. D. Nucleosome purified from (C) was then furtherly purified with Superose 6 size exclusion chromatography column.

3.3.4 Negative staining EM result of nucleosome

Negative staining EM was performed to assess the sample quality of nucleosome. The result showed that the overall shape of nucleosome was disc-like with a DNA tail that was the extranucleosomal linker DNA at one end (**Figure 25)**. The diameter of particle was estimated to be between 10 nm to 13 nm, which was consistent with the reported nucleosome diameter of 11 nm. Moreover, the EM image showed that the particles were monodisperse and had high contrast on the grid. Overall, the negative staining EM result demonstrated that the nucleosome sample was homogenous and ready for analysis by cryo-EM.

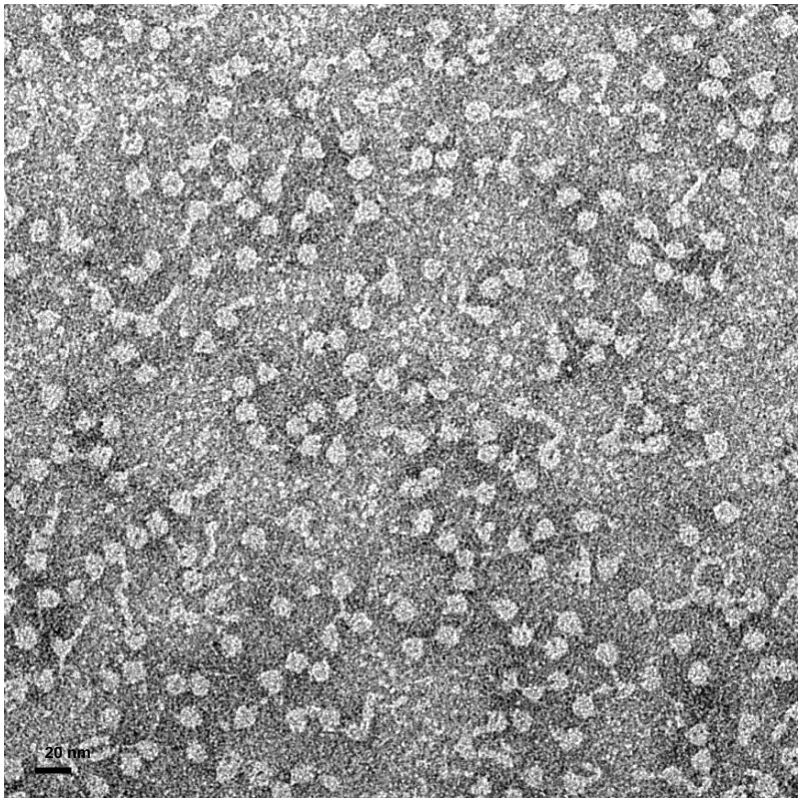

Figure 25. The negative staining EM result of nucleosome core particles.

3 µL nucleosome sample with the concentration of 80 ng/µL was pipetted on the glow-discharged holey grid and stained with 0.75% UF. The grid was observed using a 120 kV Tecnai F20 microscope (FEI) at a magnification of × 68,000. Scale bar = 20 nm.

3.3.5 Cryo-EM imaging of nucleosome

The sample of nucleosome was applied to plunge freezing for cryo-EM sample preparation. The cryo-EM image showed that the particles were monodisperse and showed little aggregation (**Figure 26)**. The particles showed high contrast on the grid. Also, the shape of nucleosome particle was consistent with negative staining EM result. Moreover, we found that some nucleosomal DNA dissociated from nucleosomes and showed long DNA strands in cryo-EM, whereas most of the nucleosomes were intact. Overall, the particle concentration, distribution and homogeneity in cryo-EM images were enough for further data collection and data processing.

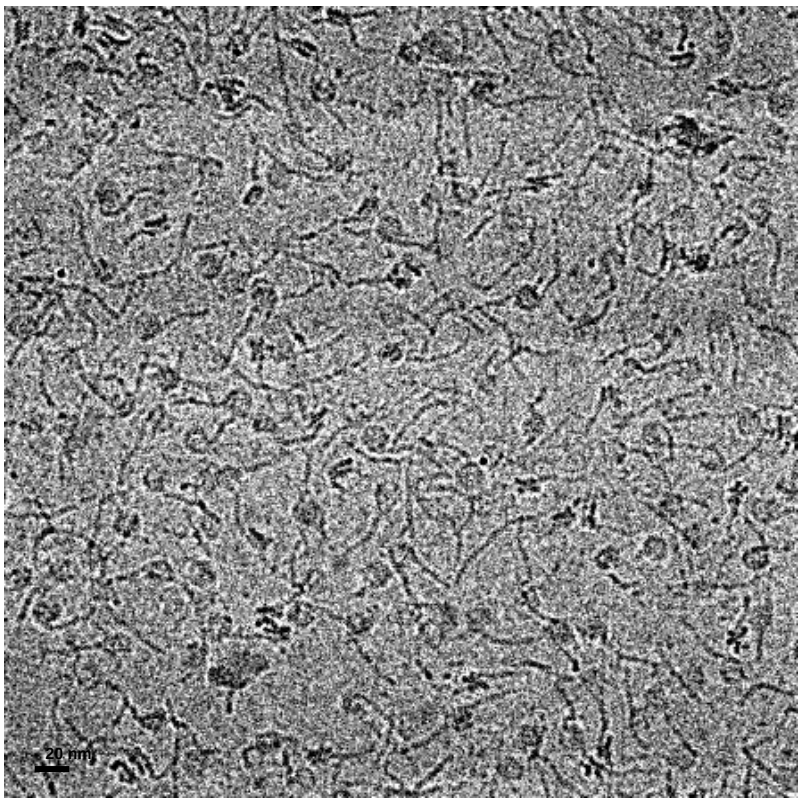

Figure 26. The cryo-EM image of nucleosome core particles (Data collected by Bob Ashley).

4 µL nucleosome sample with the concentration of 500 ng/µL was applied to a glow-discharged Quantifoil holey carbon grid. The grid was subjected to plunged freezing and observed using a Titan Krios microscope (FEI) operated at 300 kV, equipped with a Gatan K2 Summit camera. Scale bar = 20 nm.

3.3.6 Two-dimensional classification of cryo-EM nucleosome particles

After data collection, particles were picked to create the dataset. The first step of data processing for single-particle EM structure determination was two-dimensional (2D) classification, in which the dataset was aligned and grouped into some 2D homogenous subsets. After classification, some 2D subsets containing image artifacts, invalid particles, or simply empty fields, were removed. The good subsets were kept for subsequent initial structural model building. 2D classification result showed the different views of nucleosome (**Figure 27**), which were beneficial for building the model of nucleosome from various aspects. Moreover, we found that the extranucleosomal linker DNA had different angles relative to the histone octamer, which probably because the exposed DNA tail tend to move randomly due to its flexibility. This might lower the resolution of extranucleosomal linker DNA in final structural model.

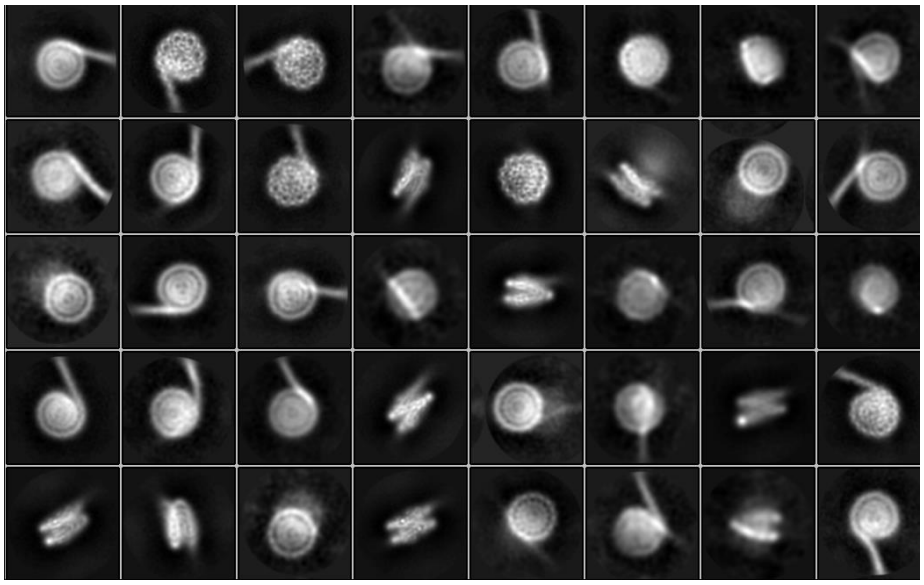

Figure 27. Two-dimensional classification of cryo-EM nucleosome particles (Data processed by Dr. Hanyong Chen).

Protein particles were picked and performed with two-dimensional classification to screen and removed bad particles. Particles were classified with different views or conformations. Data processing was performed with EMAN2 software.

3.3.7 Cryo-EM density map of nucleosome

The 2D classifications from above were applied to build the initial model of nucleosome. The cryo-EM density map of nucleosome was shown after data processing (**Figure 28A**). The structure of nucleosome from Protein Data Bank (PDB, accession number 5O9G) was fitted into the density map (**Figure 28B**). The crystal structure of histones and DNA wrapping around octamer were fitted into density map very well. The structure of extranucleosomal linker DNA did not fit with density map completely, which might be due to the flexibility of unbound extranucleosomal linker DNA. If extranucleosomal linker DNA was bound with other proteins, it would stabilize the structure of this linker DNA. In summary, our built EM model of nucleosome was consistent with the crystal structure overall, which proved our reconstituted nucleosome to be valid for application in further research.

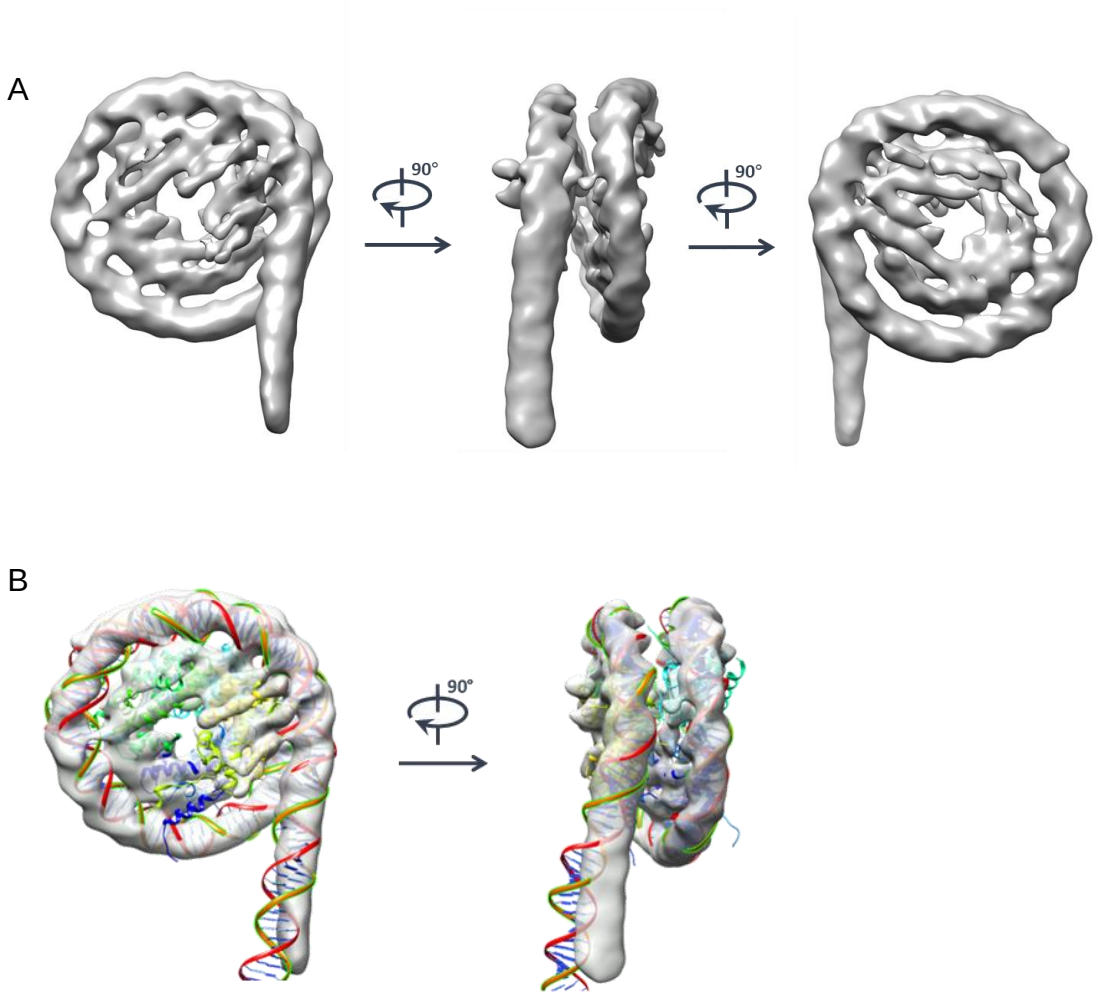

Figure 28. Cryo-EM density map of nucleosome (Data processed by Dr. Hanyong Chen).

A, Cryo-EM density map of nucleosome in different views. B, Structure of nucleosome from PDB 5O9G was fitted into EM density map.

3.4 Discussion and future directions

In Chapter 3, nucleosome was reconstituted through wrapping DNA around histone octamer refolded from purified histone proteins by salt gradient dialysis. The EM result showed that the recombinant nucleosome sample was homogenous and EM data processing achieved the initial density map of nucleosome, which was fitted by known structure of nucleosome. Nucleosome would be used for binding with SWI/SNF complex to explore remodeling mechanism in future work. The structure of nucleosome bound with remodeler would be superimposed with unbound nucleosome to identify structural difference. Moreover, nucleosome could be used for assessing biochemical activities of chromatin remodeler, including nucleosome binding ability through EMSA assay and chromatin remodeling ability through restriction-enzyme accessibility assay, as described above.

Chapter 4 Structure of catalytic subunit BRG1

4.1 Introduction

BRG1 is the essential ATPase subunit of SWI/SNF, using the energy from ATP hydrolysis to remodel nucleosomes at target regions, such as nucleosome sliding to expose target region for transcription factor binding [21]. The structure and mechanism of catalytic core domain has been identified in yeast Snf2 [46], the homologue of BRG1. As shown in **Figure 8** and discussed in Chapter 1, Snf2 binds to the SHL2 position of DNA and proximal H4 tail in nucleosome. Snf2 couples ATP hydrolysis to chromatin remodeling. The structures of Snf2 bound to the nucleosome in the presence of ADP and ADP-BeF_x have been reported [47], in which ADP-BeF_x is a non-hydrolysable ATP analogue but resembles an ATP molecule for structural analysis. In the ADP-bound state, Snf2 adopts an open conformation that is similar with the apo state (unbound state), and induces 1 bp DNA bulge at SHL2, causing the distortion of DNA. The DNA distortion propagated to the proximal end, resulting in staggered DNA translocation. In ADP-BeF_x-bound state, Snf2 triggers a closed conformation, resetting the nucleosome to a relaxed state. These findings provide the mechanism of DNA translocation regulated by Snf2 in chromatin remodeling. The catalytic core domain of *yeast Myceliophthora thermophila* MtSnf2 is ~66% and ~58% identical in sequence to *yeast Saccharomyces cerevisiae* ScSnf2 and human Brg1, respectively. The catalytic domain structure and mechanism of human BRG1 should have much similarity to yeast Snf2. Because of the key suppressive role of BRG1 on cancer development and its frequent mutation in cancers, the mechanism of human BRG1 catalytic core

domain binding to nucleosome is still deserved to be studied through detailed structural information.

The remodeling process consists of multiple steps whose precise mechanism is not completely understood until now. How the activity of catalytic subunit is regulated by its auxiliary domains remains an open question. The helicase-SANT–associated (HSA) domain is located at the N-terminus of BRG1 and has the functions of binding and cross-linking DNA. The HSA domain increases the nucleosome binding affinity and does not markedly repress the ATPase activity; instead, it downregulates the remodeling activity [45]. It was speculated that HSA may regulate a later step after ATP hydrolysis during the successive remodeling process. The HSA domain probably regulate the conformational change of ATPase domain that couples ATP hydrolysis and alters the DNA-histone contacts of the nucleosome [45]. Detailed structural information is needed to fully illustrate the regulation of remodeling by HSA domain in BRG1. Bromodomain is located at the C-terminus of BRG1 and was reported to be indispensable for the remodeling activity of BRG1 [49]. However, the function of bromodomain in BRG1 is still ambiguous. The question of how bromodomain binds to the nucleosome and regulate remodeling activity of BRG1 still needs to be fully elucidated. Although the structures of catalytic core domain, HSA domain and bromodomain have been identified respectively, as discussed in Chapter 1, the structure and mechanism of how they interact with each other and regulate the activity of catalytic subunit are still unclear. The structure of BRG1 containing these

domains bound nucleosome will certainly be valuable to explore their mechanisms of regulating chromatin remodeling.

In this chapter, we aimed to determine the structure of BRG1 protein bound with nucleosome for exploring the mechanism of remodeling activity regulated by HSA domain and bromodomain. To achieve this goal, BRG1 proteins would be purified and bound with nucleosome for remodeling. We concluded that the insect expression system was optimal for the protein expression of BRG1 catalytic core domain with high yield and purity. The optimal expression method of BRG1 proteins containing HSA domain and bromodomain would be explored in the future direction.

4.2 Materials and Methods

4.2.1 Design of truncated BRG1

Firstly, full-length BRG1 was purified from HEK 293F mammalian cells with 3 × Flag tag immunoprecipitation and the protein purity was high. However, the gel filtration result showed that most of the protein aggregated, which might result from the genomic DNA binding to BRG1 protein. Then the high salt buffer with 1 M NaCl was used to wash M2 resin to remove bound DNA. However, nearly all full-length BRG1 protein still aggregated. It was concluded that the recombinant full-length BRG1 protein was unstable to exist as monomer and tended to aggregate in vitro. Thus, the disordered sequences at the two ends of BRG1 were removed and we designed the research strategy to purify BRG1 truncations.

With sequence alignment between human BRG1 and yeast Snf2, the domain architecture of BRG1 was identified and shown in **Figure 29**. The homologous structure of catalytic core has been identified in yeast Snf2 [46]. Based on the domain architecture of BRG1, three truncations were designed; truncation 1 contained catalytic core domain; truncation 2 contained catalytic core domain and bromodomain; truncation 3 contained HSA domain, catalytic core domain and bromodomain. Each of the truncations would be expressed and purified to identify their structure and mechanism in chromatin remodeling. The structures of nucleosome bound with each BRG1 truncation would be compared to identify the structural difference caused by each domain.

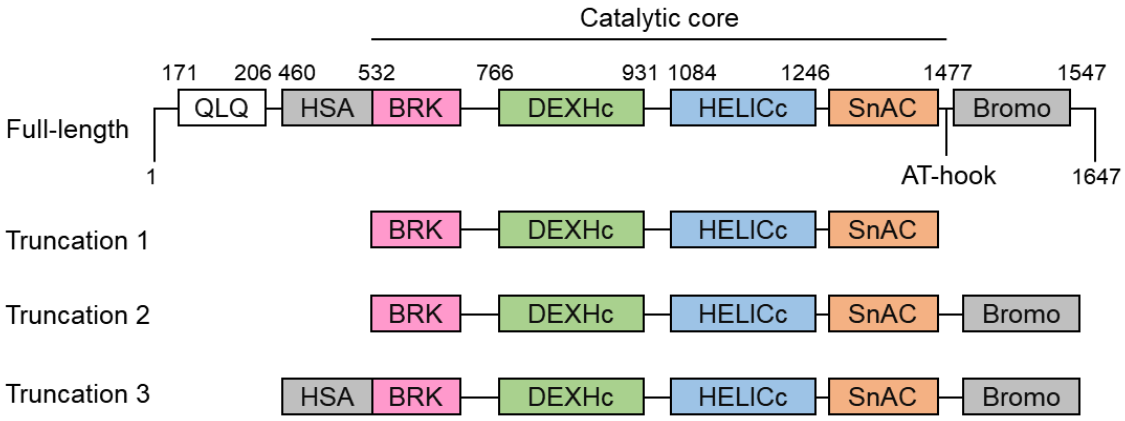

Figure 29. Design of BRG1 truncations.

Truncation 1 contains catalytic core domain of BRG1. Truncation 2 contains catalytic core domain and bromodomain. Truncation 3 contains HSA domain, catalytic core domain and bromodomain.

4.2.2 Bacteria expression system

The gene encoding BRG1 truncations were cloned into a modified pET-28a vector containing a SUMO tag and a C-terminal hexahistidine (His_6 tag), in which attached SUMO tag increased protein solubility. Constructed plasmid was transformed into Rosetta™(DE3) Competent Cells (MilliporeSigma), which was BL21 derivatives designed to enhance the expression of eukaryotic proteins that contain codons rarely used in *E. coli*. Overexpression of BRG1 was induced with 0.5 mM IPTG when an OD_{600} of 0.6-0.8 was reached. Cell culture was incubated at 16 ℃ overnight. Cells were harvested by centrifugation at 4,000 rpm for 20 min. Cell pellet was resuspended in buffer containing 50 mM HEPES, 1 M NaCl, pH 7.8, 30 mM Imidazole with lysozyme, and lysed by sonication. After a centrifugation of 12,000 rpm for 30 min, the supernatant was loaded onto an Ni-NTA column. After washing steps with washing buffer containing decreasing NaCl concentration from 1 M to 150 mM, protein was eluted with buffer containing 50 mM HEPES, 150 mM NaCl, pH 7.8, 300 mM Imidazole. The His_6-SUMO tag was cleaved with SUMO protease (Ulp) at 4 °C. Then protein sample was centrifuged to remove precipitation after Ulp cleavage and concentrated to about 500 μL. Protein was subjected to Superdex 200 10/300 size exclusion chromatography column equilibrated with 50 mM HEPES, 150 mM NaCl, pH 7.8, or an ion-exchange column. Peak fractions were collected and analyzed by SDS-PAGE.

4.2.3 Mammalian expression system

The gene encoding BRG1 truncations were cloned into a modified pcDNA3.1 vector containing a N-terminal 3 × Flag tag. Constructed plasmid was transfected

into HEK 293F suspension cells with polyethylenimine (PEI). After incubation for 72 hours at 37 °C, cells were harvested by centrifugation for 20 min at 4,000 rpm. Cells were lysed by nuclear extraction method and lysate was incubated with anti-Flag M2-agrose beads as describe above. Protein sample was eluted from resin and subjected to Superdex 200 10/300 size exclusion chromatography column for purification.

4.2.4 Insect expression system

The gene encoding BRG1 truncations with a N-terminal 3 × Flag tag were amplified from above mammalian expression plasmids by PCR, and then cloned into insect expression vector pACEBac1. The constructs containing genes of interest were transformed into DH10EMBacY competent cells for generating bacmid. The bacmid DNA was purified and transfected into Sf9 insect cells to make recombinant baculovirus as described above. The insect cell line Sf9 was cultured in serum-free conditions with suspension culture using the medium Sf-900™ III SFM. Cells were cultured in a 27°C humidified incubator. Cells were infected by baculovirus when in the mid-logarithmic phase growth and harvested 72 hours post-infection with maximum protein expression. Cells were lysed with nuclear extraction method and lysate was incubated with anti-Flag M2-agrose beads as describe above. Protein sample was eluted from resin and subjected to Superdex 200 10/300 size exclusion chromatography column for purification.

4.3 Results

4.3.1 BRG1 catalytic core domain was expressed in *E.coli* with high protein yield but less purity

Bacteria expression system was applied to express BRG1 truncations due to feasibility of large scale and less cost to get large amount of protein for structure biology. Indeed, BRG1 catalytic core domain was highly expressed in *E.coli* and efficiently eluted from Ni-NTA resin, which was used for His_6-tagged protein purification. The His_6-SUMO tag was removed by cleavage with SUMO Protease (Ulp) at 4 °C, and then the cleaved His_6-SUMO tag and Ulp were removed; however, His_6-SUMO tag and Ulp could not be separated completely from targeted protein of BRG1 catalytic core domain by gel filtration (**Figure 30**). Ion exchange chromatography with mono Q anion-exchanger and mono S cation-exchanger were also tried; however, the BRG1 catalytic core domain still could not be achieved with high purity.

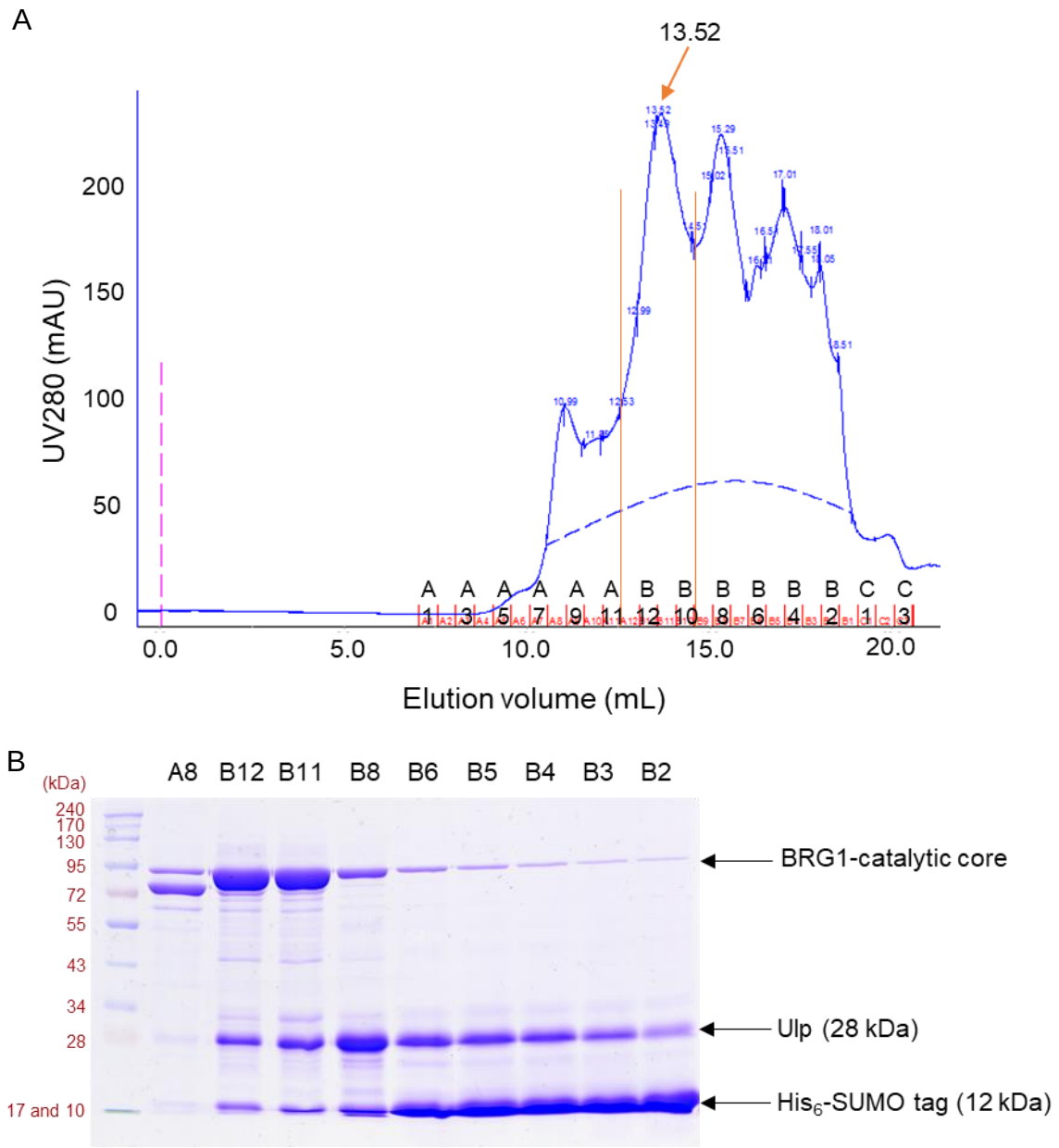

Figure 30. Protein purification result of BRG1 catalytic core domain from *E.coli*.

A, The protein of BRG1 catalytic core domain (Truncation 1) was purified from 3 liters of *E.coli* cells expressing recombinant His_6-SUMO-tagged BRG1 catalytic core domain by using Ni-NTA column. Protein sample was subjected to Superdex 200 10/300 gel filtration column after SUMO protease (Ulp) cleavage and peak was shown. B, Peak fractions were analyzed with SDS-PAGE and gel was stained with coomassie brilliant blue.

4.3.2 BRG1 catalytic core domain was expressed in HEK 293F mammalian cells with high purity but less protein yield

Mammalian cells HEK 293F was used for human BRG1 expression. All three truncations were expressed (**Figure 31**). The molecular weights of truncations were consistent with as expected. The protein of BRG1 catalytic core domain had higher purity than in *E.coli* system after gel filtration, whereas the protein yield was less (**Figure 32**). To obtain enough protein concentration (0.5-1mg/mL) for EM sample preparation, a large quantity of cells with dozens of liters of cell culture will be necessary.

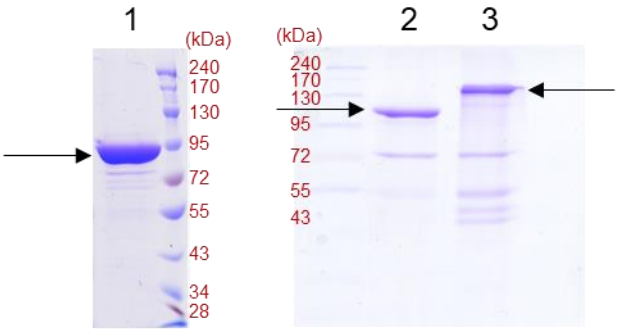

1. 3×Flag_BRG1-catalytic core (81 kDa)
2. 3×Flag_BRG1-catalytic core + Bromo (97 kDa)
3. 3×Flag_BRG1-catalytic core + Bromo + HSA (134 kDa)

Figure 31. BRG1 truncations were expressed in HEK 293F.

All three truncated BRG1 proteins were purified respectively with anti-Flag M2-agrose beads from 100 mL transfected HEK 293F cells expressing recombinant Flag-tagged proteins. Protein samples eluted from M2 beads were analyzed with SDS-PAGE and gels were stained with coomassie brilliant blue.

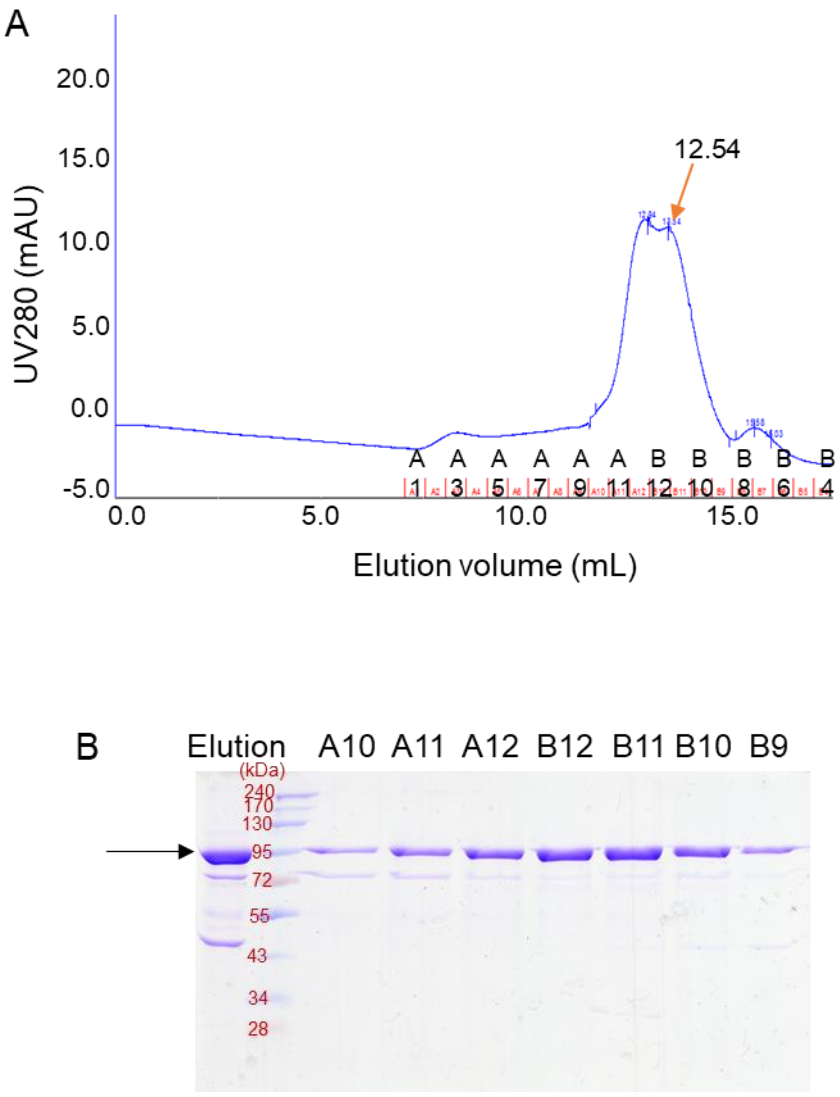

Figure 32. Protein purification result of BRG1 catalytic core domain from HEK 293F. A, Protein of BRG1 catalytic core domain (Truncation 1) was purified with anti-Flag M2-agrose beads from 1 liter of transfected HEK 293F cells expressing recombinant Flag-tagged BRG1 catalytic core domain. Protein sample eluted from M2 beads was subjected to Superdex 200 10/300 gel filtration column and peak was shown. The OD280 value of peak was 11 mAu. B, Peak fractions were analyzed with SDS-PAGE and gel was stained with coomassie brilliant blue. The arrow indicated the protein band of BRG1 catalytic core domain.

4.3.3 BRG1 catalytic core domain was expressed in Sf9 insect cells with high purity and high protein yield

Insect cell line Sf9 was used to express protein with baculovirus expression system. Although Sf9 is not mammalian expression system, it still can provide a eukaryotic expression environment. As shown in **Figure 33**, the expression level of BRG1 catalytic core domain was much higher than in HEK 293F, and the protein yield was about 7 times of the yield in HEK 293F. Moreover, the protein purity in Sf9 was much improved than in *E.coli* and HEK 293F. In summary, Sf9 insect expression system was optimal for protein expression and purification of BRG1 catalytic core domain. However, the other two BRG1 truncations did not express well in Sf9 cells. Truncation 2 (BRG1-catalytic core + Bromo) showed low expression, whereas truncation 3 (BRG1-catalytic core + Bromo + HSA) does not show expression that could be detected by coomassie brilliant blue staining.

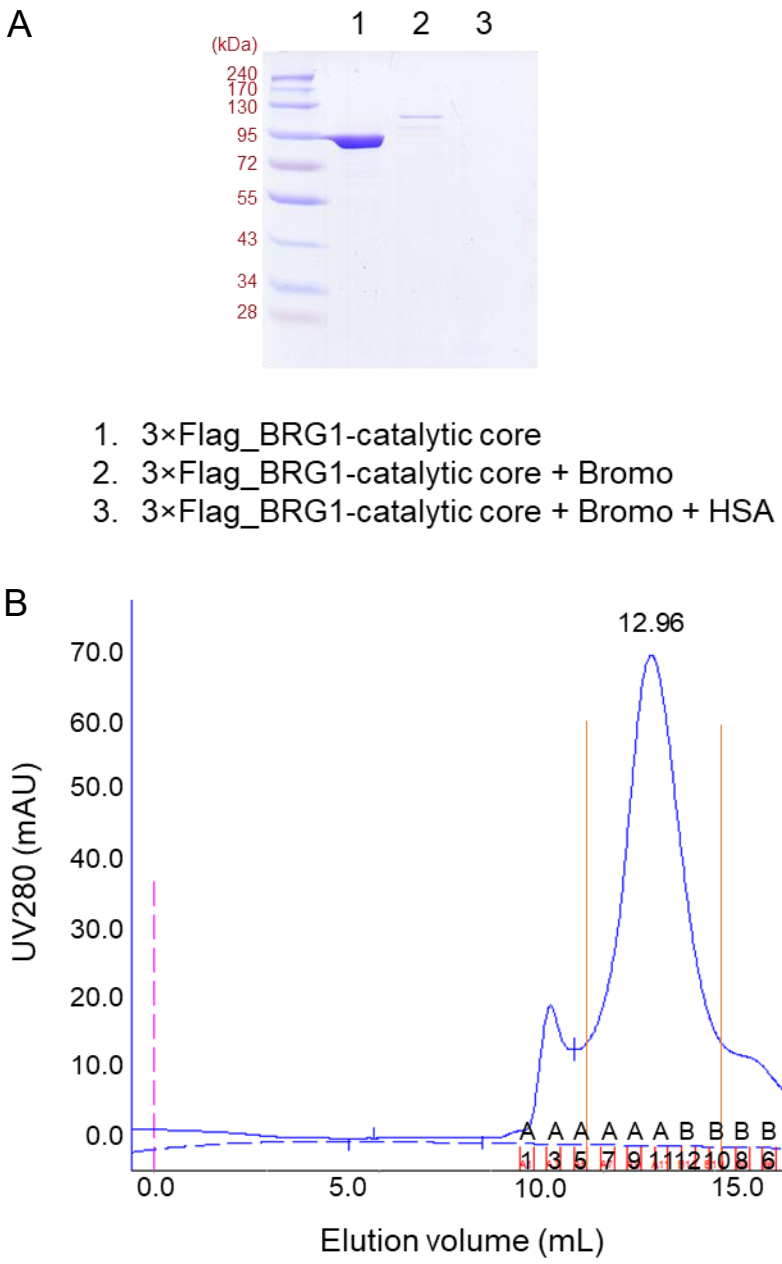

Figure 33. Protein purification result of BRG1 catalytic core domain from Sf9 cells.

A, All three truncated BRG1 proteins were purified respectively from baculovirus-infected Sf9 cells expressing recombinant Flag-tagged BRG1 truncations. Protein samples eluted from M2 beads were analyzed with SDS-PAGE and gel was stained with coomassie brilliant blue. B, Protein of BRG1 catalytic core domain (Truncation 1) purified from 1 liter of baculovirus-infected Sf9 cells was subjected to Superdex 200 10/300 gel filtration column and peak was shown. The OD280 value of peak was 70 mAu.

4.4 Discussion and future directions

In Chapter 4, truncated BRG1 protein was expressed and purified to study the structure and mechanism of BRG1 domains in chromatin remodeling. To achieve the protein sample with high yield and purity, three different expression systems commonly used in structural biology were applied and the results indicated that Sf9 insect expression system was the best way to purify the protein of BRG1 catalytic core domain. However, the other two BRG1 truncations (BRG1-catalytic core + Bromo and BRG1-catalytic core + Bromo + HSA) did not express well in Sf9. Although these two truncations showed decent expression in HEK 293F cells, their expression amount were much less than truncation 1 (BRG1-catalytic core). This is probably because these two truncations are degraded in cells. These two truncations would be designed with modification to improve expression.

In future work, protein of BRG1 catalytic core domain would be bound with reconstituted nucleosome to study the chromatin remodeling mechanism through EM. Even though human BRG1 is conserved with yeast Snf2, we still cannot exclude the possibility that some detailed structure or mechanism may have difference. Due to the key suppressive role of BRG1 on cancer development and its frequent mutation in cancers, the mechanism of human BRG1 catalytic core domain in chromatin remodeling is still deserved to be studied through detailed structural information, which would contribute to the research of BRG1-mutant cancer.

Bibliography

1. Venkatesh, S. and J.L. Workman, *Histone exchange, chromatin structure and the regulation of transcription.* Nat Rev Mol Cell Biol, 2015. **16**(3): p. 178-89.
2. Fyodorov, D.V., et al., *Emerging roles of linker histones in regulating chromatin structure and function.* Nat Rev Mol Cell Biol, 2018. **19**(3): p. 192-206.
3. Hergeth, S.P. and R. Schneider, *The H1 linker histones: multifunctional proteins beyond the nucleosomal core particle.* EMBO Rep, 2015. **16**(11): p. 1439-53.
4. Clapier, C.R. and B.R. Cairns, *The biology of chromatin remodeling complexes.* Annu Rev Biochem, 2009. **78**: p. 273-304.
5. Becker, P.B. and J.L. Workman, *Nucleosome remodeling and epigenetics.* Cold Spring Harb Perspect Biol, 2013. **5**(9).
6. Valencia, A.M. and C. Kadoch, *Chromatin regulatory mechanisms and therapeutic opportunities in cancer.* Nat Cell Biol, 2019. **21**(2): p. 152-161.
7. Peterson, C.L. and I. Herskowitz, *Characterization of the yeast SWI1, SWI2, and SWI3 genes, which encode a global activator of transcription.* Cell, 1992. **68**(3): p. 573-83.
8. Tamkun, J.W., et al., *brahma: a regulator of Drosophila homeotic genes structurally related to the yeast transcriptional activator SNF2/SWI2.* Cell, 1992. **68**(3): p. 561-72.
9. Kwon, H., et al., *Nucleosome disruption and enhancement of activator binding by a human SW1/SNF complex.* Nature, 1994. **370**(6489): p. 477-81.
10. Vignali, M., et al., *ATP-dependent chromatin-remodeling complexes.* Mol Cell Biol, 2000. **20**(6): p. 1899-910.
11. Cairns, B.R., et al., *RSC, an essential, abundant chromatin-remodeling complex.* Cell, 1996. **87**(7): p. 1249-60.
12. Tang, L., E. Nogales, and C. Ciferri, *Structure and function of SWI/SNF chromatin remodeling complexes and mechanistic implications for transcription.* Prog Biophys Mol Biol, 2010. **102**(2-3): p. 122-8.
13. Martens, J.A. and F. Winston, *Recent advances in understanding chromatin remodeling by Swi/Snf complexes.* Curr Opin Genet Dev, 2003. **13**(2): p. 136-42.
14. Mohrmann, L. and C.P. Verrijzer, *Composition and functional specificity of SWI2/SNF2 class chromatin remodeling complexes.* Biochim Biophys Acta, 2005. **1681**(2-3): p. 59-73.
15. Kadoch, C. and G.R. Crabtree, *Mammalian SWI/SNF chromatin remodeling complexes and cancer: Mechanistic insights gained from human genomics.* Sci Adv, 2015. **1**(5): p. e1500447.
16. Masliah-Planchon, J., et al., *SWI/SNF chromatin remodeling and human malignancies.* Annu Rev Pathol, 2015. **10**: p. 145-71.
17. Wilson, B.G. and C.W. Roberts, *SWI/SNF nucleosome remodellers and cancer.* Nat Rev Cancer, 2011. **11**(7): p. 481-92.
18. Helming, K.C., X. Wang, and C.W.M. Roberts, *Vulnerabilities of mutant SWI/SNF complexes in cancer.* Cancer Cell, 2014. **26**(3): p. 309-317.

19. Phelan, M.L., et al., *Reconstitution of a core chromatin remodeling complex from SWI/SNF subunits.* Mol Cell, 1999. **3**(2): p. 247-53.
20. DelBove, J., et al., *Identification of a core member of the SWI/SNF complex, BAF155/SMARCC1, as a human tumor suppressor gene.* Epigenetics, 2011. **6**(12): p. 1444-53.
21. Trotter, K.W. and T.K. Archer, *The BRG1 transcriptional coregulator.* Nucl Recept Signal, 2008. **6**: p. e004.
22. Mashtalir, N., et al., *Modular Organization and Assembly of SWI/SNF Family Chromatin Remodeling Complexes.* Cell, 2018. **175**(5): p. 1272-1288 e20.
23. Ho, L., et al., *An embryonic stem cell chromatin remodeling complex, esBAF, is essential for embryonic stem cell self-renewal and pluripotency.* Proc Natl Acad Sci U S A, 2009. **106**(13): p. 5181-6.
24. Narayanan, R., et al., *Loss of BAF (mSWI/SNF) Complexes Causes Global Transcriptional and Chromatin State Changes in Forebrain Development.* Cell Rep, 2015. **13**(9): p. 1842-54.
25. Yan, L., et al., *Structural Insights into BAF47 and BAF155 Complex Formation.* J Mol Biol, 2017. **429**(11): p. 1650-1660.
26. Sen, P., et al., *Loss of Snf5 Induces Formation of an Aberrant SWI/SNF Complex.* Cell Rep, 2017. **18**(9): p. 2135-2147.
27. Schiaffino-Ortega, S., et al., *SWI/SNF proteins as targets in cancer therapy.* J Hematol Oncol, 2014. **7**: p. 81.
28. Lu, C. and C.D. Allis, *SWI/SNF complex in cancer.* Nat Genet, 2017. **49**(2): p. 178-179.
29. Kadoch, C., et al., *Proteomic and bioinformatic analysis of mammalian SWI/SNF complexes identifies extensive roles in human malignancy.* Nat Genet, 2013. **45**(6): p. 592-601.
30. Chun, H.E., et al., *Genome-Wide Profiles of Extra-cranial Malignant Rhabdoid Tumors Reveal Heterogeneity and Dysregulated Developmental Pathways.* Cancer Cell, 2016. **29**(3): p. 394-406.
31. Versteege, I., et al., *Truncating mutations of hSNF5/INI1 in aggressive paediatric cancer.* Nature, 1998. **394**(6689): p. 203-6.
32. Wang, X., et al., *SMARCB1-mediated SWI/SNF complex function is essential for enhancer regulation.* Nat Genet, 2017. **49**(2): p. 289-295.
33. Helming, K.C., et al., *ARID1B is a specific vulnerability in ARID1A-mutant cancers.* Nat Med, 2014. **20**(3): p. 251-4.
34. Chandler, R.L., et al., *ARID1a-DNA interactions are required for promoter occupancy by SWI/SNF.* Mol Cell Biol, 2013. **33**(2): p. 265-80.
35. Poynter, S.T. and C. Kadoch, *Polycomb and trithorax opposition in development and disease.* Wiley Interdiscip Rev Dev Biol, 2016. **5**(6): p. 659-688.
36. Stanton, B.Z., et al., *Smarca4 ATPase mutations disrupt direct eviction of PRC1 from chromatin.* Nat Genet, 2017. **49**(2): p. 282-288.
37. Kadoch, C., et al., *Dynamics of BAF-Polycomb complex opposition on heterochromatin in normal and oncogenic states.* Nat Genet, 2017. **49**(2): p. 213-222.

38. Nakayama, R.T., et al., *SMARCB1 is required for widespread BAF complex-mediated activation of enhancers and bivalent promoters.* Nat Genet, 2017. **49**(11): p. 1613-1623.
39. Pan, J., et al., *Interrogation of Mammalian Protein Complex Structure, Function, and Membership Using Genome-Scale Fitness Screens.* Cell Syst, 2018. **6**(5): p. 555-568 e7.
40. Kim, K.H., et al., *SWI/SNF-mutant cancers depend on catalytic and non-catalytic activity of EZH2.* Nat Med, 2015. **21**(12): p. 1491-6.
41. Smith, C.L., et al., *Structural analysis of the yeast SWI/SNF chromatin remodeling complex.* Nat Struct Biol, 2003. **10**(2): p. 141-5.
42. Dechassa, M.L., et al., *Architecture of the SWI/SNF-nucleosome complex.* Mol Cell Biol, 2008. **28**(19): p. 6010-21.
43. Zhang, Z., et al., *Architecture of SWI/SNF chromatin remodeling complex.* Protein Cell, 2018. **9**(12): p. 1045-1049.
44. Schubert, H.L., et al., *Structure of an actin-related subcomplex of the SWI/SNF chromatin remodeler.* Proc Natl Acad Sci U S A, 2013. **110**(9): p. 3345-50.
45. Xia, X., et al., *Structure of chromatin remodeler Swi2/Snf2 in the resting state.* Nat Struct Mol Biol, 2016. **23**(8): p. 722-9.
46. Liu, X., et al., *Mechanism of chromatin remodelling revealed by the Snf2-nucleosome structure.* Nature, 2017. **544**(7651): p. 440-445.
47. Li, M., et al., *Mechanism of DNA translocation underlying chromatin remodelling by Snf2.* Nature, 2019. **567**(7748): p. 409-413.
48. Shen, W., et al., *Solution structure of human Brg1 bromodomain and its specific binding to acetylated histone tails.* Biochemistry, 2007. **46**(8): p. 2100-10.
49. Morrison, E.A., et al., *DNA binding drives the association of BRG1/hBRM bromodomains with nucleosomes.* Nat Commun, 2017. **8**: p. 16080.
50. Medina, P.P. and M. Sanchez-Cespedes, *Involvement of the chromatin-remodeling factor BRG1/SMARCA4 in human cancer.* Epigenetics, 2008. **3**(2): p. 64-8.
51. Orvis, T., et al., *BRG1/SMARCA4 inactivation promotes non-small cell lung cancer aggressiveness by altering chromatin organization.* Cancer Res, 2014. **74**(22): p. 6486-6498.
52. Roy, N., et al., *Brg1 promotes both tumor-suppressive and oncogenic activities at distinct stages of pancreatic cancer formation.* Genes Dev, 2015. **29**(6): p. 658-71.
53. Bai, J., et al., *BRG1 is a prognostic marker and potential therapeutic target in human breast cancer.* PLoS One, 2013. **8**(3): p. e59772.
54. Raab, J.R., et al., *Co-regulation of transcription by BRG1 and BRM, two mutually exclusive SWI/SNF ATPase subunits.* Epigenetics Chromatin, 2017. **10**(1): p. 62.
55. Hoffman, G.R., et al., *Functional epigenetics approach identifies BRM/SMARCA2 as a critical synthetic lethal target in BRG1-deficient cancers.* Proc Natl Acad Sci U S A, 2014. **111**(8): p. 3128-33.
56. Oike, T., et al., *A synthetic lethality-based strategy to treat cancers harboring a genetic deficiency in the chromatin remodeling factor BRG1.* Cancer Res, 2013. **73**(17): p. 5508-18.

57. Passmore, L.A. and C.J. Russo, *Specimen Preparation for High-Resolution Cryo-EM.* Methods Enzymol, 2016. **579**: p. 51-86.
58. Irons, S.L., et al., *Protein Production Using the Baculovirus Expression System.* Curr Protoc Protein Sci, 2018. **91**: p. 5 5 1-5 5 22.
59. Sohn, D.H., et al., *SRG3 interacts directly with the major components of the SWI/SNF chromatin remodeling complex and protects them from proteasomal degradation.* J Biol Chem, 2007. **282**(14): p. 10614-24.
60. Keppler, B.R. and T.K. Archer, *Ubiquitin-dependent and ubiquitin-independent control of subunit stoichiometry in the SWI/SNF complex.* J Biol Chem, 2010. **285**(46): p. 35665-74.
61. Wang, H.W. and J.W. Wang, *How cryo-electron microscopy and X-ray crystallography complement each other.* Protein Sci, 2017. **26**(1): p. 32-39.
62. Harris, J.R. and S. De Carlo, *Negative staining and cryo-negative staining: applications in biology and medicine.* Methods Mol Biol, 2014. **1117**: p. 215-58.
63. Meister, A. and A. Blume, *(Cryo)Transmission Electron Microscopy of Phospholipid Model Membranes Interacting with Amphiphilic and Polyphilic Molecules.* Polymers (Basel), 2017. **9**(10).
64. Dobro, M.J., et al., *Plunge freezing for electron cryomicroscopy.* Methods Enzymol, 2010. **481**: p. 63-82.
65. Stark, H., *GraFix: stabilization of fragile macromolecular complexes for single particle cryo-EM.* Methods Enzymol, 2010. **481**: p. 109-26.
66. Kim, D.N. and K.Y. Sanbonmatsu, *Tools for the cryo-EM gold rush: going from the cryo-EM map to the atomistic model.* Biosci Rep, 2017. **37**(6).
67. Cutter, A.R. and J.J. Hayes, *A brief review of nucleosome structure.* FEBS Lett, 2015. **589**(20 Pt A): p. 2914-22.
68. Luger, K., et al., *Characterization of nucleosome core particles containing histone proteins made in bacteria.* J Mol Biol, 1997. **272**(3): p. 301-11.
69. Lowary, P.T. and J. Widom, *New DNA sequence rules for high affinity binding to histone octamer and sequence-directed nucleosome positioning.* J Mol Biol, 1998. **276**(1): p. 19-42.
70. Dyer, P.N., et al., *Reconstitution of nucleosome core particles from recombinant histones and DNA.* Methods Enzymol, 2004. **375**: p. 23-44.
71. Luger, K., T.J. Rechsteiner, and T.J. Richmond, *Preparation of nucleosome core particle from recombinant histones.* Methods Enzymol, 1999. **304**: p. 3-19.